SAE 4320 Case Core Composite Steel Iteration #63

MICROSTRUCTURAL DATA, MONOTONIC AND FATIGUE TEST RESULTS

F. Yin and A. Fatemi

Department of Mechanical, Industrial, and
Manufacturing Engineering
The University of Toledo
Toledo, OH 43606

Prepared for:

The AISI Bar Steel Applications Group

October 2003

NOMENCLATURE

A_o, A_f	initial, final area	S	engineering stress
HB, HRB, HRC	Brinell, Rockwell B-Scale, Rockwell C-Scale hardness number	YS, UYS, LYS, YS'	monotonic yield, upper yield, lower yield, cyclic yield strength
b, c, n	fatigue strength, fatigue ductility, strain hardening exponent	YPE	yield point elongation
D_o, D_f	initial, final diameter	S_u	ultimate tensile strength
e	engineering strain	%EL	percent elongation
E, E'	monotonic, midlife cycle modulus of elasticity	%RA	percent reduction in area
K, K'	monotonic, cyclic strength coefficient	σ, σ_f, σ_f'	true stress, true fracture strength, fatigue strength coefficient
L_o, L_f	initial, final gage length	σ_a, σ_m, $\Delta\sigma$	stress amplitude, mean stress, stress range
$N_{50\%}$, $(N_f)_{10\%}$, $(N_f)_{50\%}$,	number of cycles to midlife, 10% load drop, 50% load drop	ε_e, ε_p, ε	true elastic, plastic, total strain
$2N_f$	reversals to failure	ε_f, ε_f'	true fracture ductility, fatigue ductility coefficient
P_f, P_u	fracture, ultimate load	ε_a, ε_m, $\Delta\varepsilon$	strain amplitude, mean strain, strain range
R	neck radius; or strain ratio	$\Delta\varepsilon_e$, $\Delta\varepsilon_p$	elastic, plastic strain range

TABLE OF CONTENTS

UNIT CONVERSION TABLE

Measure	SI Unit	US Unit	from SI to US	from US to SI
Length	mm	in	1 mm = 0.03937 in	1 in = 25.4 mm
Area	mm^2	in^2	1 mm^2 = 0.00155 in^2	1 in^2 = 645.16 mm^2
Load	kN	klb	1kN = 0.2248 klb	1 klb = 4.448 kN
Stress	MPa	ksi	1 MPa = 0.14503 ksi	1 ksi = 6.895 MPa
Temperature	°C	°F	°C = (°F - 32)/1.8	°F = (°C * 1.8) + 32

In SI Unit:

1 kN = 10^3 N 1 Pa = 1 N/m^2 1 MPa = 10^6 Pa = 1 N/mm^2 1 Gpa = 10^9 Pa

In US Unit:

1 klb = 10^3 lb 1 psi = 1 lb/in^2 1 ksi = 10^3 psi

SUMMARY

The monotonic properties, and fatigue behavior data have been obtained for SAE 4320 Case-Core Composite steel. The material was provided by Timken Company. Two tensile tests were performed to acquire the desired monotonic properties. Eighteen fatigue tests were performed to obtain the strain-life and cyclic stress-strain curves and properties. The experimental procedure followed and results obtained are presented and discussed in this report.

I. EXPERIMENTAL PROGRAM

1.1 Material and Specimen Fabrication

1.1.1 Material

The SAE 4320 Case Core steel was provided by Timken Company. This material was delivered to the University of Toledo in round bar form. The bars were approximately 1 inch in diameter. In Table 1, the chemical composition is shown. The hardness profile is shown in Figure 1b.

1.1.2 Specimen

In this study, identical round specimens were used for the monotonic and fatigue tests. The specimen configuration and dimensions are shown in Figure 1a. This configuration deviates slightly from the specimens recommended by ASTM Standard E606 [1]. The recommended specimens have uniform or hourglass test sections. The specimen geometry shown in Figure 1a differs by using a large secondary radius throughout the test section.

All specimens were machined in the Mechanical, Industrial, and Manufacturing Engineering Machine Shop at the University of Toledo. The specimens were cut to the appropriate length, after that center-drilled in both ends and inserted into a CNC machine. Using the CNC machine, specimens were rough machined, then heat treated and ground.

A commercial round-specimen polishing machine was used to polish the specimen gage section. Three different grits of aluminum oxide lapping film were used: 15μ, 9μ, and 3μ. The 3μ grit was used as the final polish and polishing marks coincided

with the specimens' longitudinal direction. The polished surfaces were carefully examined under magnification to ensure complete removal of machine marks within the test section.

1.2 Testing Equipment

1.2.1 Apparatus

An INSTRON 8801 closed-loop servo-hydraulic axial load frame in conjunction with a Fast-Track digital servo-controller was used to conduct the tests. The calibration of this system was verified prior to beginning the test program. The load cell used had a capacity of 11 klb. Hydraulically operated grips using universal tapered collets were employed to secure the specimens' ends in series with the load cell.

Total strain was controlled for all tests using an extensometer rated as ASTM class B1 [2]. The calibration of the extensometer was verified using displacement apparatus containing a micrometer barrel in divisions of 0.0001 in. The extensometer had a gage length of 0.30 in and was capable of measuring strains up to 15 %.

In order to protect the specimens' surface from the knife-edges of the extensometer, ASTM Standard E606 recommends the use of transparent tape or epoxy to 'cushion' the attachment. For this study, it was found that application of transparent tape strips was difficult due to the radius within the test section. Therefore, epoxy was considered to be the best protection. One disadvantage of epoxy is the variability of mixtures throughout the test program. As an alternative to epoxy, M-coat D offered a more consistent mixture. Therefore, the tests were performed using M-coat D.

All tests were conducted at room temperature and were monitored using a digital thermometer. In order to minimize temperature effects upon the extensometer and load cell calibrations, fluctuations were maintained within ± 2 °C (± 3.6 °F) as required by ASTM Standard E606. Also, the relative humidity of the air was monitored using a precision hydrometer.

1.2.2 Alignment

Significant effort was put forth to align the load train (load cell, grips, specimen, and actuator). Misalignment can result from both tilt and offset between the central lines of the load train components. According to ASTM Standard E606, the maximum bending strains should not exceed 5 % of the minimum axial strain range imposed during any test program. For this study, the minimum axial strain range was 0.0070 in/in. Therefore, the maximum allowable bending strain was 350 microstrain. ASTM Standard E1012, Type A, Method 1 was followed to verify specimen alignment [3]. For this procedure, two arrays of four strain gages per array were arranged at the upper and lower ends of the uniform gage section. For each array, gages were equally spaced around the circumference of a 0.5-in. uniform diameter bar. The maximum bending strain determined from the gaged specimen was less than 60 microstrain. This value was well within the allowable ASTM limit.

1.3 Test Methods and Procedures

1.3.1 Monotonic tension tests

All monotonic tests in this study were performed using test methods specified by ASTM Standard E8 [4]. Two specimens were used to obtain the monotonic properties. Strain control was used until fracture.

For the elastic and initial yield region (0% to 0.5% strain), a strain rate of 0.0025 in/in/min was chosen. This strain rate was three-quarters of the maximum allowable rate specified by ASTM Standard E8 for the initial yield region. After yielding (0.5% strain to fracture), the strain rate was increased by a factor of three (i.e., 0.0075 in/in/min).

After the tension tests were concluded, the broken specimens were carefully reassembled. The final gage lengths of the fractured specimens were measured with a Vernier caliper having divisions of 0.001 in. Using an optical comparator with 10X magnification and divisions of 0.001 in, the final diameter and the neck radius were measured. It should be noted that prior to the test, the initial minimum diameter was measured with this same instrument.

1.3.2 Constant amplitude fatigue tests

All constant amplitude fatigue tests in this study were performed according to ASTM Standard E606. It is recommended by this standard that at least 10 specimens be used to generate the fatigue properties. For this study, 18 specimens at 6 different strain amplitudes ranging from 0.35% to 2% were utilized. Instron LCF software was used in all tests, except for the tests done in load control and displacement control (in which Instron

SAX software was used). During each test, the total strain was recorded using the extensometer output. Test data were automatically recorded throughout each test.

There were three control modes used for these tests. Strain control was used in the tests with plastic deformation (2%, 1.3%, 1% and 0.5% strain amplitudes), for two of the three tests at 0.5% strain amplitude, load control was used for the remainder of the tests to prevent high mean stress. Displacement control was used in three of the higher level tests (2% and 1.3%) to free the specimen surface inside gage length, so replicas could be taken to detect short cracks during fatigue tests. First displacement amplitude was monitored in these three tests during strain control, then the same displacement amplitude was used in the displacement control test. For all the elastic tests (0.4% and 0.35% strain amplitudes) strain control was used initially to determine the stabilized load, then load control was used for the remainder of the tests. For the tests starting with strain control, the applied frequencies ranged from 0.1 Hz to 2 Hz in order to keep a strain rate about 0.02 in/in/sec. For the load control tests, the frequency was increased between 2 Hz and 26 Hz in order to shorten the overall test duration. All strain control tests were conducted using a triangular waveform. Displacement amplitudes were monitored during all the tests. Plot of strain amplitude vs. displacement amplitude is shown in Figure A.4, from which one can see in elastic region this relation is linear and in plastic region this relation is nonlinear.

II. EXPERIMENTAL RESULTS AND ANALYSIS

2.1 Microstructural Data

Photomicrographs of the microstructure were obtained using an optical microscope with a digital camera attachment. In Figure 2, the transverse direction is shown for case, core and transition area at 500X magnification. It can be seen from this photomicrograph that SAE 4320 Case-Core composite steel had a martensite microstructure. In Figure 3, the inclusions/voids in T'-T direction are shown at 100X magnification. For Figures 2 and 3, the rolling direction is perpendicular to the page.

According to ASTM Standard E45, method A, the inclusion rating number for type A inclusion in T'-T direction was found [6]. Residual stresses were also measured. The residual stress profile is shown in Figure A.3b. A summary of the microstructural data for SAE 4320 Case-Core Composite steel is provided in Table 2.

2.2 Monotonic Deformation Behavior

The properties determined from monotonic tests were the following: modulus of elasticity (E), yield strength (YS), ultimate tensile strength (S_u), percent elongation (%EL), percent reduction in area (%RA), true fracture strength (σ_f), true fracture ductility (ε_f), strength coefficient (K), and strain hardening exponent (n).

True stress (σ), true strain (ε), and true plastic strain (ε_p) were calculated from engineering stress (S) and engineering strain (e), according to the following relationships which are based on constant volume assumption:

$$\sigma = S(1+e) \tag{1a}$$

$$\varepsilon = \ln(1+e) \tag{1b}$$

$$\varepsilon_p = \varepsilon - \varepsilon_e = \varepsilon - \frac{\sigma}{E} \tag{1c}$$

The true stress (σ) - true strain (ε) plot is often represented by the Ramberg-Osgood equation:

$$\varepsilon = \varepsilon_e + \varepsilon_p = \frac{\sigma}{E} + \left(\frac{\sigma}{K}\right)^{\frac{1}{n}} \tag{2}$$

The strength coefficient, K, and strain hardening exponent, n, are the intercept and slope of the best line fit to true stress (σ) versus true plastic strain (ε_p) data in log-log scale:

$$\sigma = K\left(\varepsilon_p\right)^n \tag{3}$$

In accordance with ASTM Standard E739 [7], when performing the least squares fit, the true plastic strain (ε_p) was the independent variable and the stress (σ) was the dependent variable. This plot for the test conducted is shown in Figure 4. To generate the K and n values, the range of data used in this figure was chosen according to the definition of discontinuous yielding specified in ASTM Standard E646 [8]. Therefore, the valid data range occurred between the end of yield point extension and the strain at or prior to maximum load.

The true fracture strength, σ_f, was corrected for necking according to the Bridgman correction factor [9]:

$$\sigma_f = \frac{\frac{P_f}{A_f}}{\left(1 + \frac{4R}{D_f}\right) \ln\left(1 + \frac{D_f}{4R}\right)} \quad (4)$$

where P_f is the load at fracture, R is the neck radius, and D_f is the diameter at fracture.

The true fracture ductility, ε_f, was calculated from the relationship based on constant volume:

$$\varepsilon_f = \ln\left(\frac{A_o}{A_f}\right) = \ln\left(\frac{1}{1 - RA}\right) \quad (5)$$

where A_f is the cross-sectional area at fracture, A_o is the original cross-sectional area, and RA is the reduction in area.

A summary of the monotonic properties for SAE 4320 Case-Core Composite steel is provided in Table 2. The monotonic stress-strain curves for two tests are shown in Figure 5. As can be seen from this figure, the two curves for the composite case-core material are close to each other. Refer to Table A.1 in the Appendix for a summary of the monotonic test results.

2.3 Cyclic Deformation Behavior

2.3.1 Transient cyclic response

Transient cyclic response describes the process of cyclic-induced change in deformation resistance of a material. Data obtained from constant amplitude strain-controlled fatigue tests were used to determine this response. Plots of stress amplitude

variation versus applied number of cycles can indicate the degree of transient cyclic softening/hardening. Also, these plots show when cyclic stabilization occurs. A composite plot of the transient cyclic response for SAE 4320 Case-Core Composite steel is shown in Figure A.1 of the Appendix. The transient response is normalized on the rectangular plot in Figure A.1a, while a semi-log plot is shown in Figure A.1c. Mean stress response is normalized on the rectangular plot in Figure A.1b, while a semi-log plot for mean stresses is shown in Figure A.1d. Even though multiple tests were conducted at each strain amplitude, data from one test at each strain amplitude tested are shown in these plots.

2.3.2 Steady-state cyclic deformation

Another cyclic behavior of interest was the steady state or stable response. Data obtained from constant amplitude strain-controlled fatigue tests were also used to determine this response. The properties determined from the steady-state hysteresis loops were the following: cyclic modulus of elasticity (E'), cyclic strength coefficient (K'), cyclic strain hardening exponent (n'), and cyclic yield strength (YS'). Half-life (midlife) hysteresis loops and data were used to obtain the stable cyclic properties.

Similar to monotonic behavior, the cyclic true stress-strain behavior can be characterized by the Ramberg-Osgood type equation:

$$\frac{\Delta \varepsilon}{2} = \frac{\Delta \varepsilon_e}{2} + \frac{\Delta \varepsilon_p}{2} = \frac{\Delta \sigma}{2E} + \left(\frac{\Delta \sigma}{2K'} \right)^{\frac{1}{n'}} \qquad (6)$$

It should be noted that in Equation 6 and the other equations that follow, E is the average modulus of elasticity that was calculated from the monotonic tests.

The cyclic strength coefficient, K', and cyclic strain hardening exponent, n', are the intercept and slope of the best line fit to true stress amplitude ($\Delta\sigma/2$) versus true plastic strain amplitude ($\Delta\varepsilon_p/2$) data in log-log scale:

$$\frac{\Delta\sigma}{2} = K'\left(\frac{\Delta\varepsilon_p}{2}\right)^{n'} \tag{7}$$

In accordance with ASTM Standard E739, when performing the least squares fit, the true plastic strain amplitude ($\Delta\varepsilon_p/2$) was the independent variable and the stress amplitude ($\Delta\sigma/2$) was the dependent variable. The true plastic strain amplitude was calculated by the following equation:

$$\frac{\Delta\varepsilon_p}{2} = \frac{\Delta\varepsilon}{2} - \frac{\Delta\sigma}{2E} \tag{8}$$

This plot is shown in Figure 6. To generate the K' and n' values, the range of data used in the figure was chosen for $[\Delta\varepsilon_p/2]_{\text{calculated}} \geq 0.0020$ in/in.

The cyclic stress - strain curve reflects the resistance of a material to cyclic deformation and can be vastly different from the monotonic stress - strain curve. The cyclic stress - strain curves of the composite and case and core materials are shown in Figure 7. In Figure 8, superimposed plots of monotonic and cyclic curves are shown. As can be seen in Figure 8, SAE 4320 Case-Core Composite steel cyclically softens. Figure A.2 in the Appendix shows a composite plot of the steady-state (midlife) hysteresis loops. Even though multiple tests were conducted at each strain amplitude, the stable loops from only one test at each strain amplitude are shown in this plot.

2.4 Constant Amplitude Fatigue Behavior

Constant amplitude strain-controlled fatigue tests were performed to determine the strain-life curve. The following equation relates the true strain amplitude to the fatigue life:

$$\frac{\Delta \varepsilon}{2} = \frac{\Delta \varepsilon_e}{2} + \frac{\Delta \varepsilon_p}{2} = \frac{\sigma_f'}{E}\left(2N_f\right)^b + \varepsilon_f'\left(2N_f\right)^c \qquad (9)$$

where σ_f' is the fatigue strength coefficient, b is the fatigue strength exponent, ε_f' is the fatigue ductility coefficient, c is the fatigue ductility exponent, E is the monotonic modulus of elasticity, and $2N_f$ is the number of reversals to failure (which was defined as a 50% tensile load drop, as recommended by ASTM Standard E606).

The fatigue strength coefficient, σ_f', and fatigue strength exponent, b, are the intercept and slope of the best line fit to true stress amplitude ($\Delta\sigma/2$) versus reversals to failure ($2N_f$) data in log-log scale:

$$\frac{\Delta \sigma}{2} = \sigma_f'\left(2N_f\right)^b \qquad (10)$$

In accordance with ASTM Standard E739, when performing the least squares fit, the stress amplitude ($\Delta\sigma/2$) was the independent variable and the reversals to failure ($2N_f$) was the dependent variable. This plot is shown in Figure 9. To generate the σ_f' and b values, the range of data used in this figure was chosen for $N_f \leq 10^6$ cycles.

The fatigue ductility coefficient, ε_f', and fatigue ductility exponent, c, are the intercept and slope of the best line fit to calculated true plastic strain amplitude ($\Delta\varepsilon_p/2$) versus reversals to failure ($2N_f$) data in log-log scale:

$$\left(\frac{\Delta\varepsilon_p}{2}\right)_{calculated} = \varepsilon_f^{'}\left(2N_f\right)^C \tag{11}$$

In accordance with ASTM Standard E739, when performing the least squares fit, the calculated true plastic strain amplitude ($\Delta\varepsilon_p/2$) was the independent variable and the reversals to failure ($2N_f$) was the dependent variable. The calculated true plastic strain amplitude was determined from Equation 8. This plot is shown in Figure 10. To generate the ε_f' and c values, the range of data used in this figure was chosen for $[\Delta\varepsilon_p/2]_{\text{calculated}} \geq$ 0.0020 in/in. Replicas were taken inside the gage length of the specimen surface every 10% of failure life for two fatigue tests conducted by displacement control. No evidence of short cracks was found in the replicas.

The true strain amplitude versus reversals to failure plot is shown in Figure 11. This plot displays the strain - life curve (Eqn. 9), the elastic strain portion (Eqn. 10), the plastic strain portion (Eqn. 11), and superimposed fatigue data. Subsurface failure occurred for tests where $\varepsilon_a \leq 0.5\%$, as indicated in Table A.2, and a typical photo is shown in Figure A.3a. A summary of the cyclic properties for SAE 4320 Case-Core Composite steel is provided in Table 2. Table A.2 in the Appendix provides the summary of the fatigue test results. Superimposed curves with case, core and case-core composite are shown in Figure A.5 to Figure A.10. It can be clearly seen in Figures A.5 to Figure A.9 that all of the case-core composite curves lie in between the case and core curves as expected. It can also be seen from the strain-life curves shown in Figure A.10 that in the low-cycle fatigue region the case-core composite curve lies in between the case and core curves, while in high-cycle fatigue region it merge with the case curve.

Table 1: Chemical composition of SAE 4320 steel
(obtained from University of Waterloo report for Iteration 50 for the case material)

Element	Wt. %
Carbon, C	0.18%
Manganese, Mn	0.48%
Phosphorus, P	0.006%
Sulfur, S	0.02%
Silicon, Si	0.26%
Copper, Cu	0.17%
Nickel, Ni	1.74%
Chromium, Cr	0.58%
Molybdenum, Mo	0.17%
Tin, Sn	NA
Aluminum, Al	NA
Vanadium, V	NA
Nitrogen, N	NA
Titanium, Ti	NA
Niobium, Nb	NA
Tellurium, Te	NA

Table 2: Summary of the Mechanical Properties

Microstructural Data	Average
ASTM grain size number (MAG=500X):	
The transverse direction (T'-T)	2 to 3
Inclusion rating number (MAG=100X):	
Type A (sulfide type), thin series	2 to 2.5
Type B (alumina type), thin series	None
Type C (silicate type), thin series	None
Type D (globular type), thin series	None
Hardness:	
Brinell (HB)	
Transverse direction (T-T')	NA
The first longitudinal direction (L-T)	NA
Rockwell B-scale (HRB)	
Transverse direction (T-T')	NA
The first longitudinal direction (L-T)	NA
Rockwell C-scale (HRC)	
Transverse direction (T-T')	56 on the surface, 44 at the center (See hardness profile in Fig. 1b)
The first longitudinal direction (L-T)	NA
Microstructure type:	
The first longitudinal direction (L-T)	martensite

Monotonic Properties	Average		Range	
Modulus of elasticity, E, GPa (ksi):	201.2	(29,176.2)	200.2 - 202.1	(29,036.4 - 29,316.0)
Yield strength (0.2% offset), YS , MPa (ksi):	1344.5	(195.0)	1335.9 - 1353.1	(193.8 - 196.3)
Upper yield strength UYS, MPa (ksi):	NA			
Lower yield strength LYS, MPa (ksi):	NA			
Yield point elongation, YPE (%):	NA			
Ultimate strength, S_u , MPa (ksi):	1705.3	(247.3)	1692.2 - 1718.5	(245.4 - 249.2)
Percent elongation, %EL (%):	32.0%		30.3% - 33.7%	
Percent reduction in area, %RA (%):	55.5%		54.2% - 56.9%	
Strength coefficient, K , MPa (ksi):	2,343.8	(339.9)	2,331.8 - 2,355.8	(338.2 - 341.7)
Strain hardening exponent, n:	0.0840		0.0838 - 0.0842	
True fracture strength, σ_f *, MPa (ksi):	2197.8	(318.7)	2184.2 - 2211.3	(316.8 - 320.7)
True fracture ductility, ε_f (%):	81.1%		78.0% - 84.1%	

Cyclic Properties	Average		Range	
Cyclic modulus of elasticity, E' , GPa (ksi):	194.9	(28,259.9)	182.7 - 206.0	(26,492.3 - 29,872.1)
Fatigue strength coefficient, σ_f' , MPa (ksi):	2,306.1	(334.5)		
Fatigue strength exponent, b:	-0.0752			
Fatigue ductility coefficient, ε_f' :	0.1427			
Fatigue ductility exponent, c:	-0.4738			
Cyclic yield strength, YS', MPa (ksi)	1220.2	(177.0)		
Cyclic strength coefficient, K' , MPa (ksi):	2,636.4	(382.4)		
Cyclic strain hardening exponent, n':	0.1240			
Fatigue strength @ 10^6 cycles, S_f, Mpa (ksi)	774.5	(112.3)		

* Correction was made according to the Bridgman correction factor.

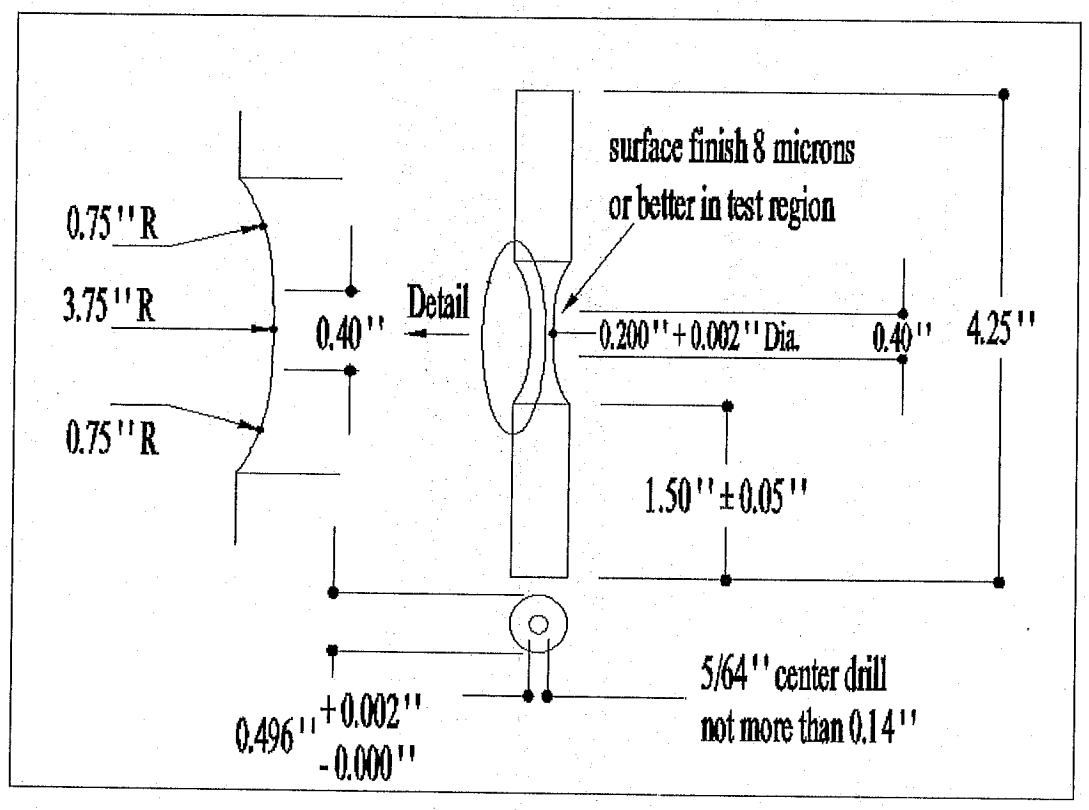

Figure 1a: Specimen configuration and dimensions

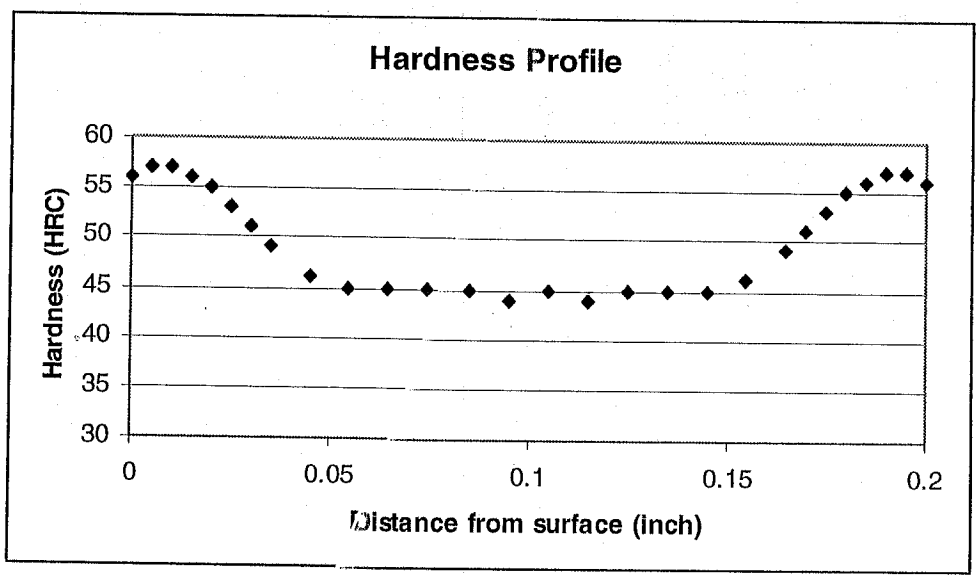

Figure 1b: Hardness profile (measured by Daimler Chrysler)

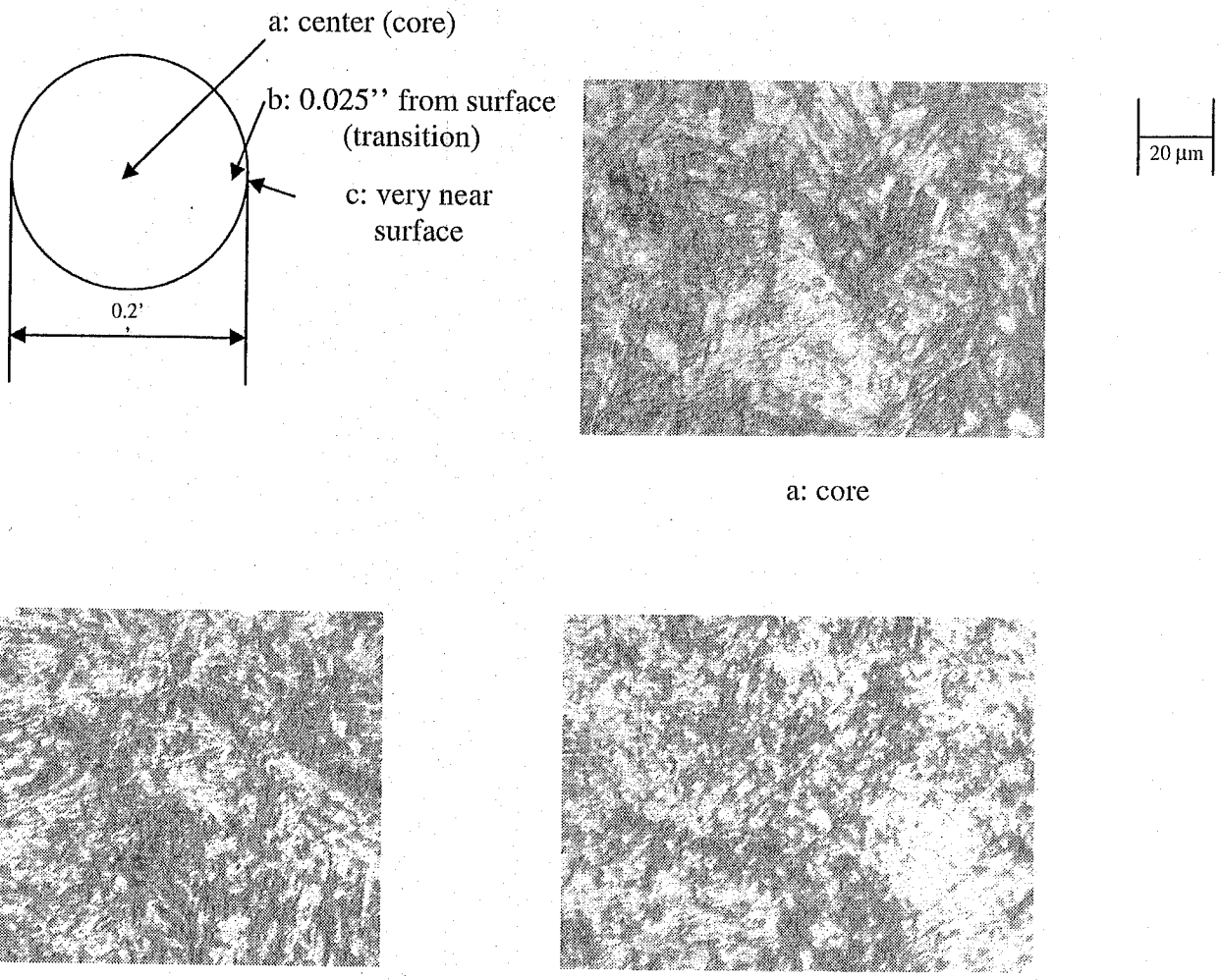

Figure 2: Photomicrograph in transverse direction (T'-T) at 500X for SAE 4320 Case-Core Composite steel (rolling direction is perpendicular)

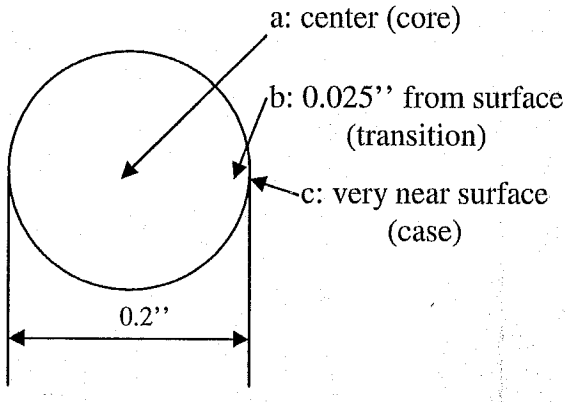

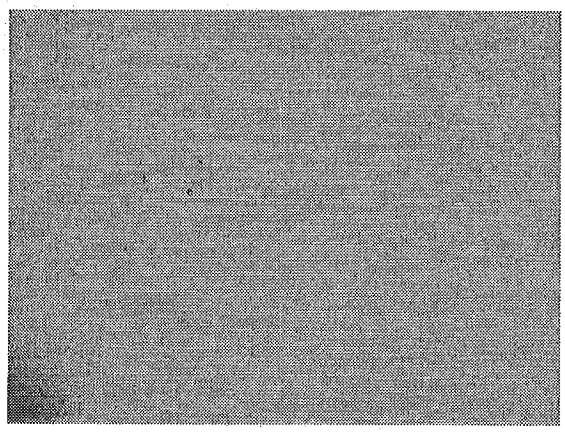

a: core

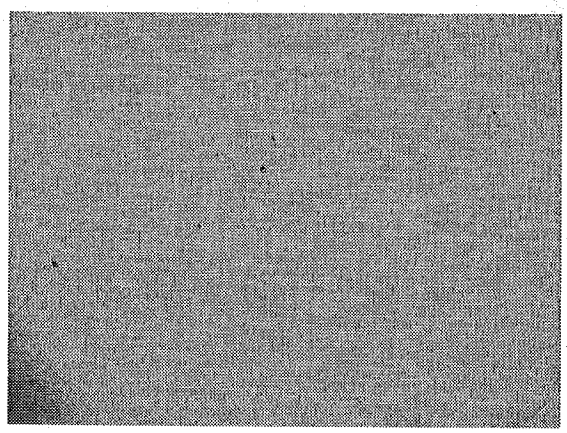

b: transition

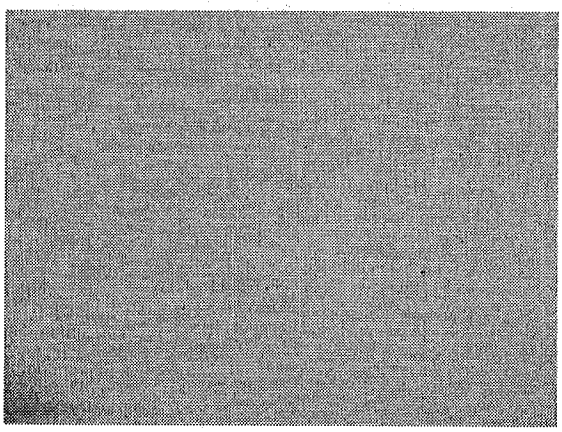

c: case

Figure 3: Examples of inclusions in the transverse direction (T'-T) at 100X for SAE 4320 Case-Core Composite steel (rolling direction is perpendicular)

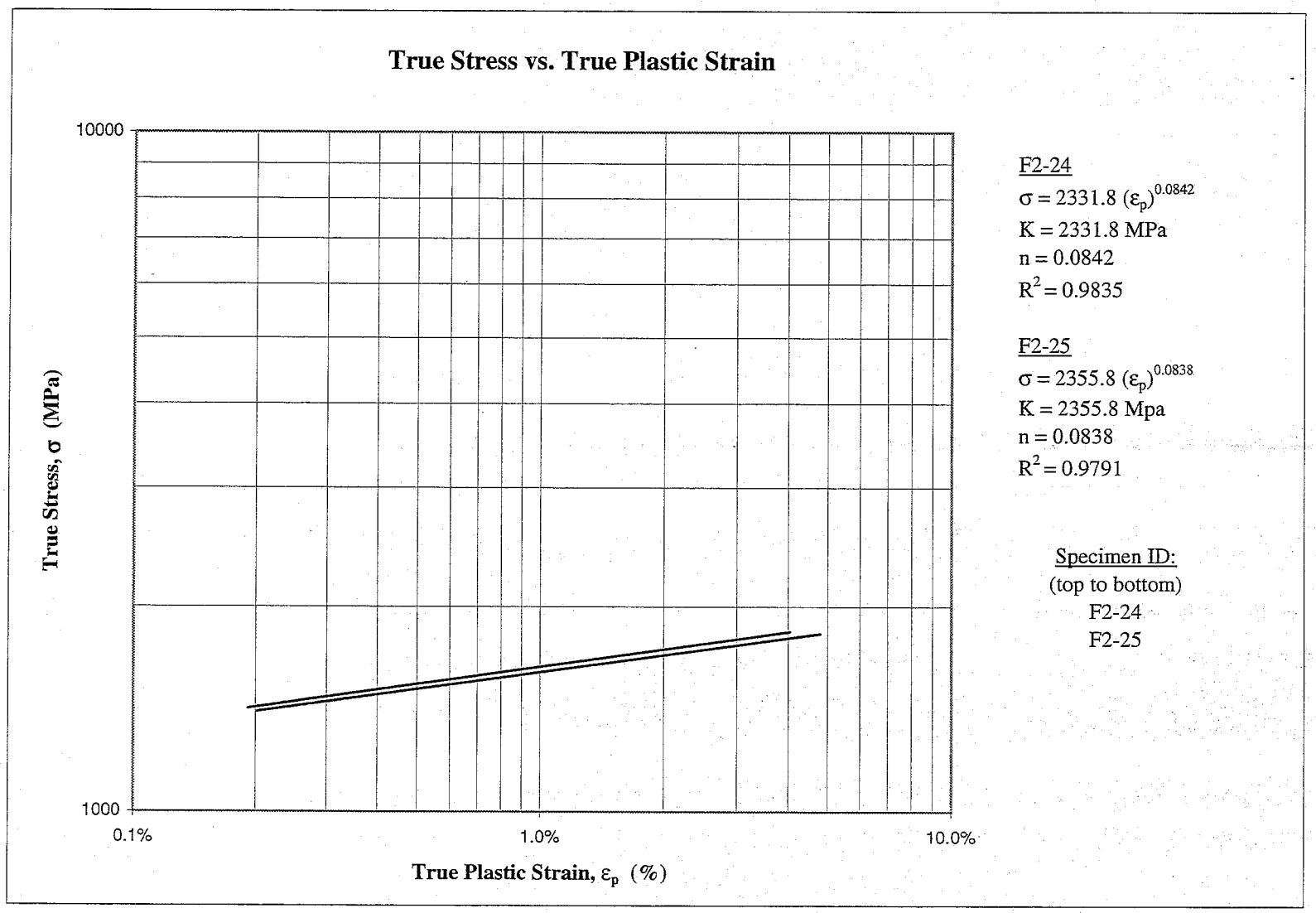

Figure 4: True stress versus true plastic strain

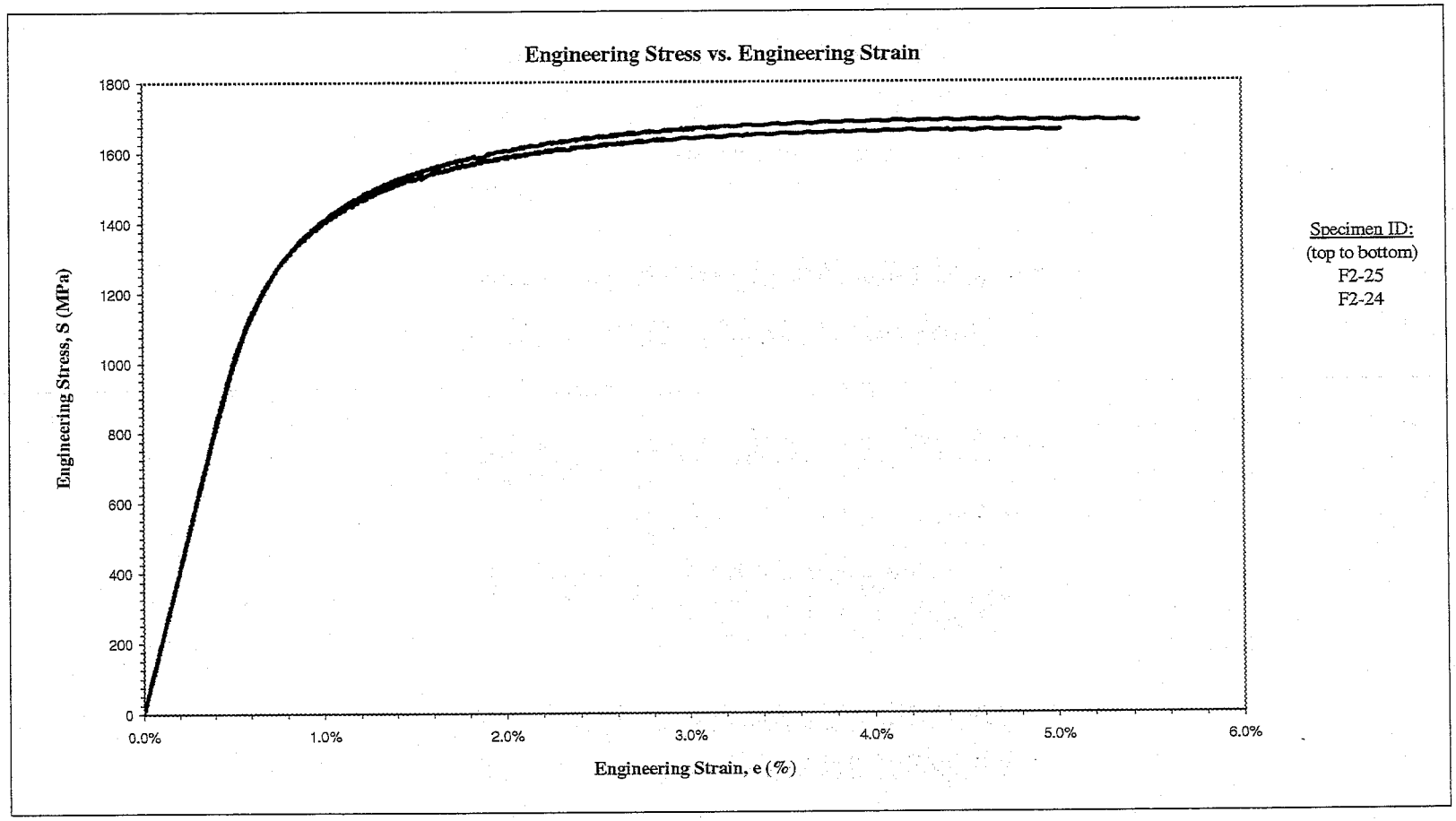

Figure 5: Monotonic stress-strain curves

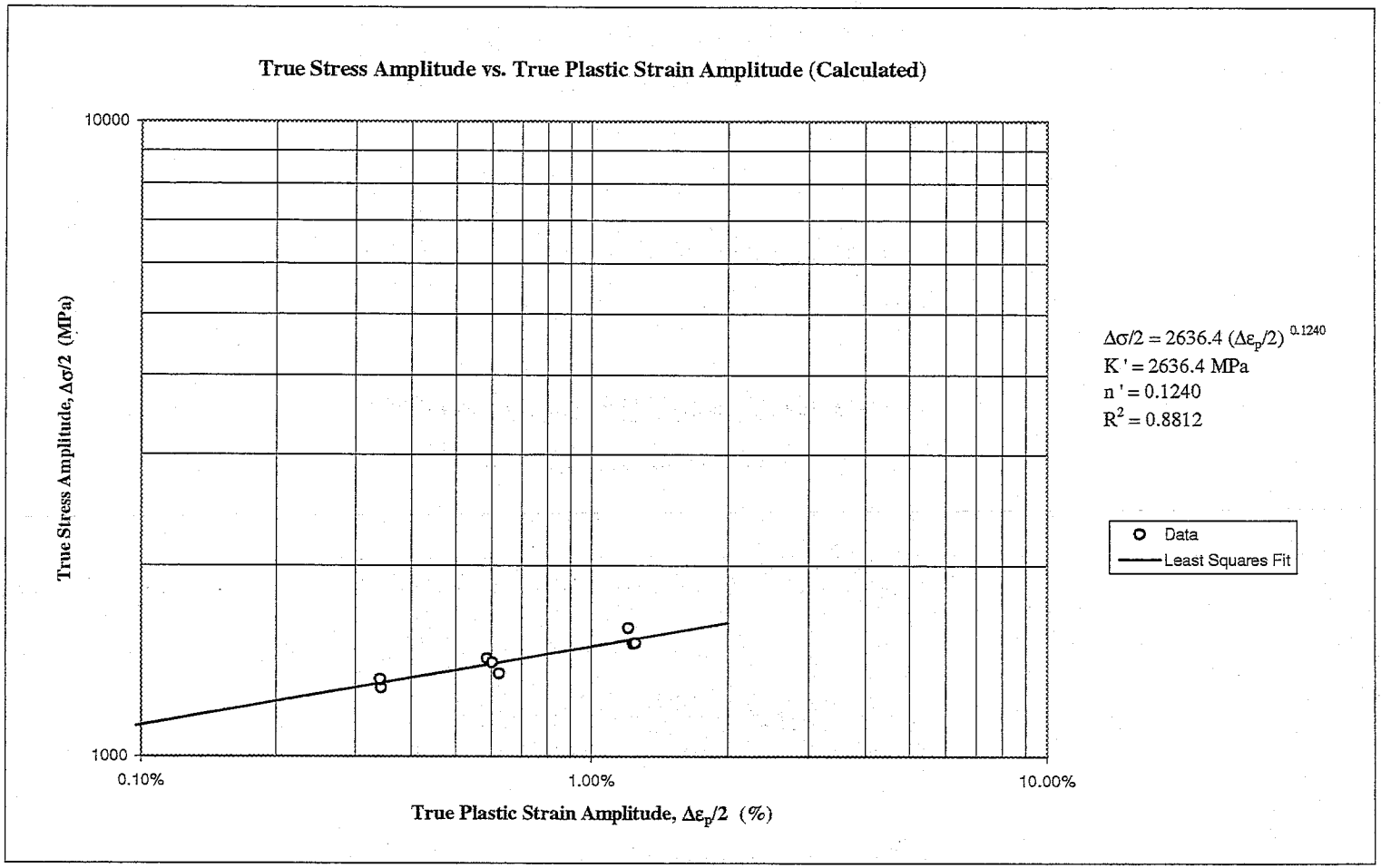

Figure 6: True stress amplitude versus calculated true plastic strain amplitude

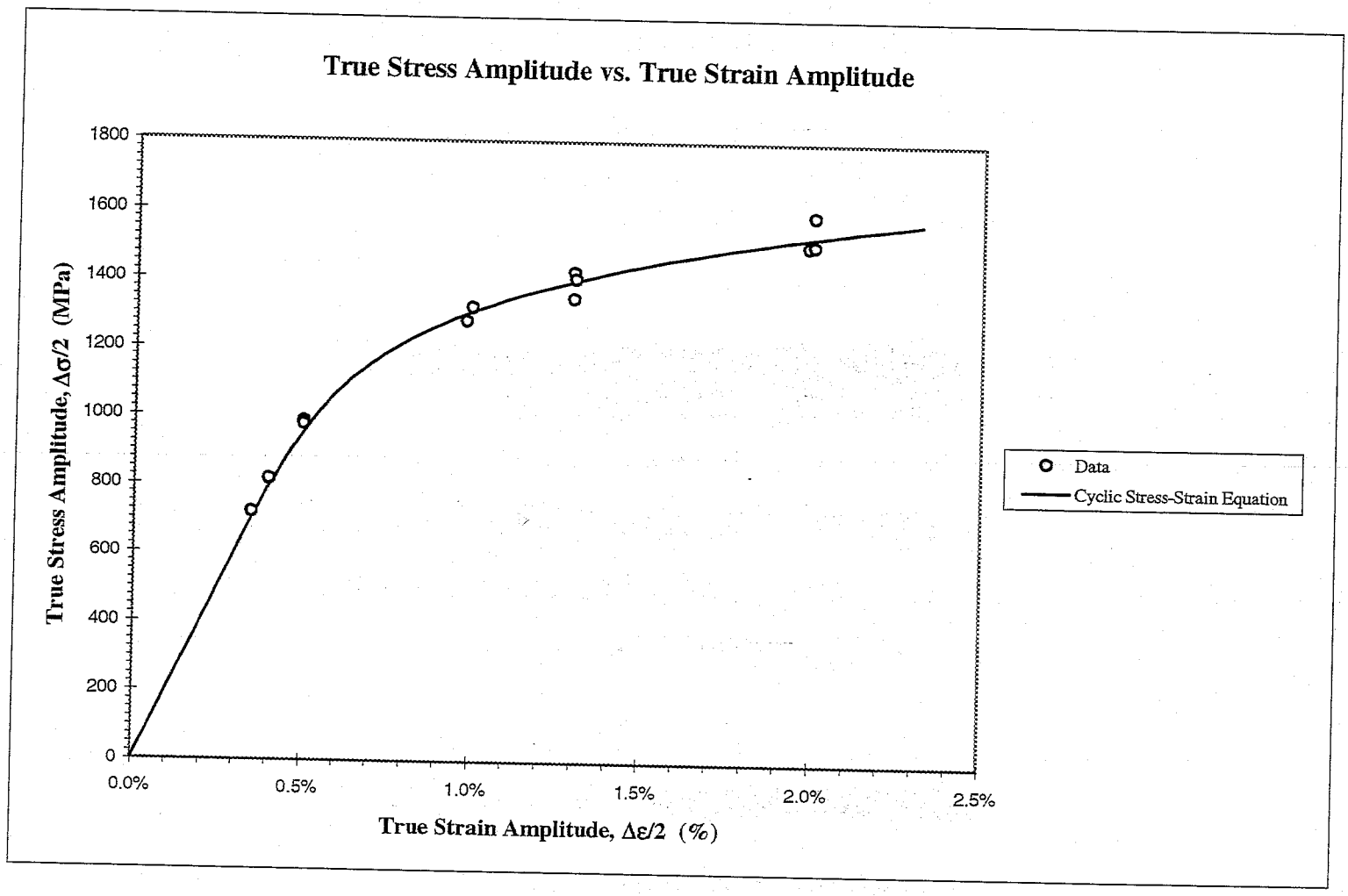

Figure 7: True stress amplitude versus true strain amplitude

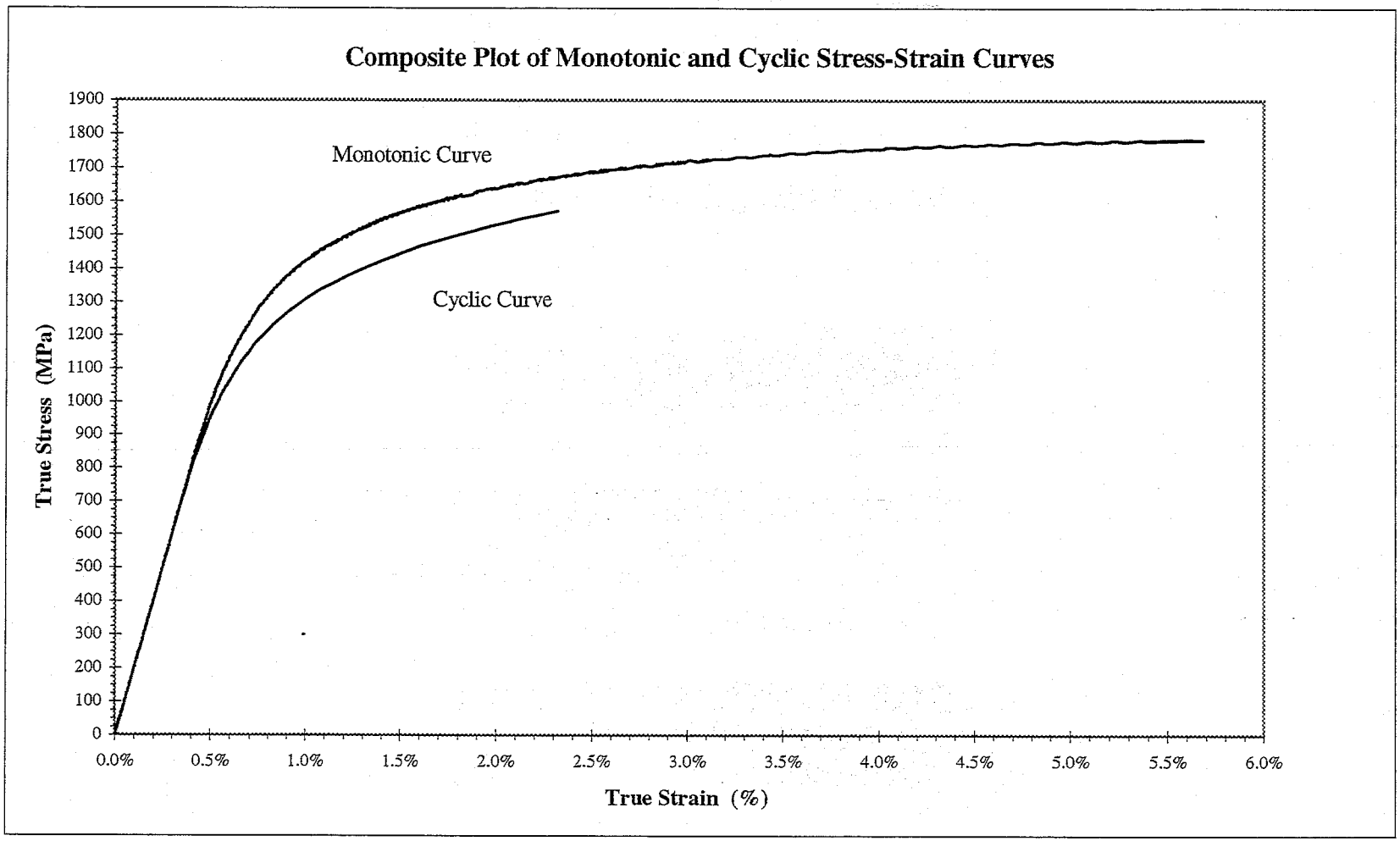

Figure 8: Composite plot of cyclic and monotonic stress-strain curves

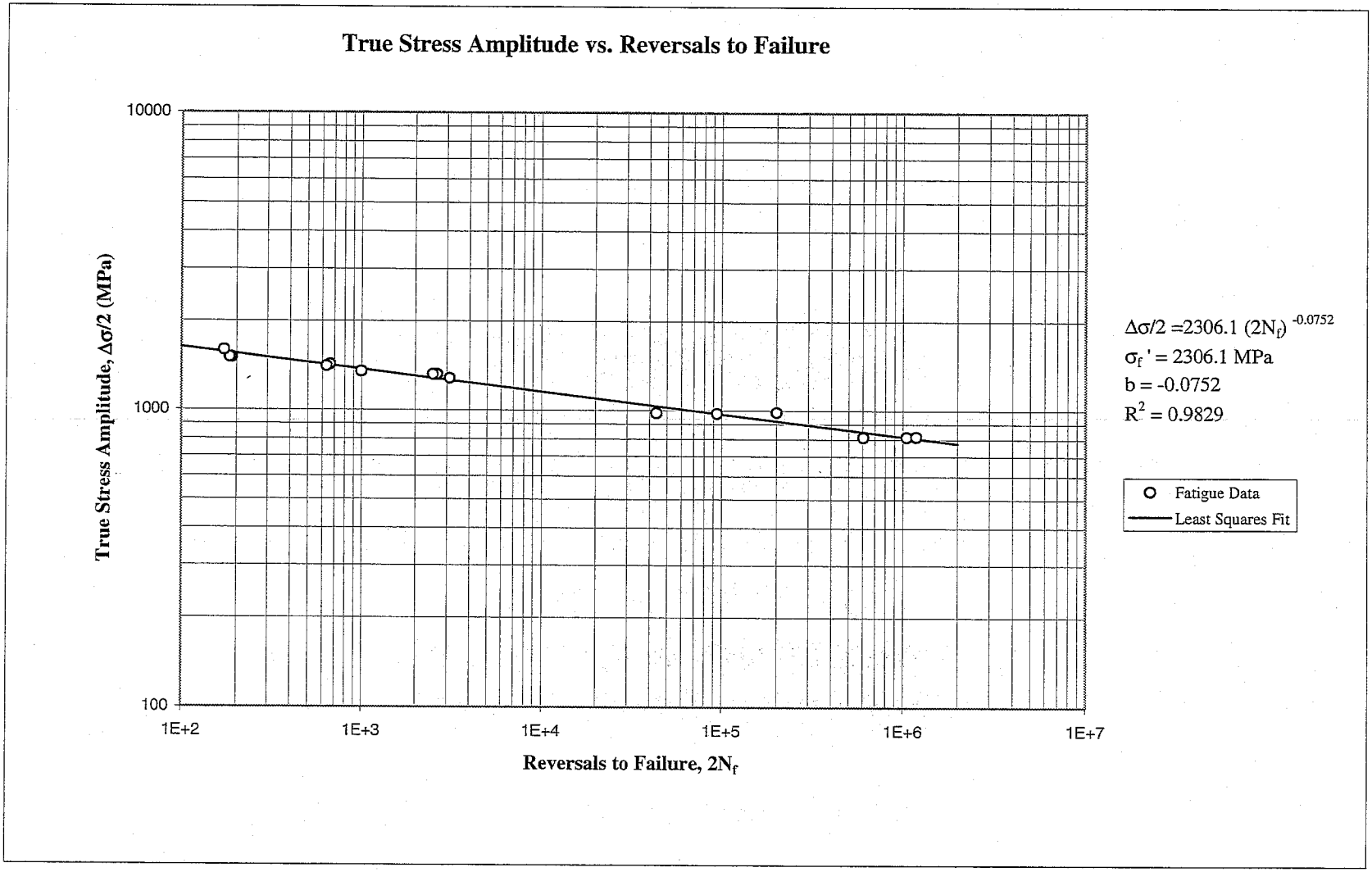

Figure 9: True stress amplitude versus reversals to failure

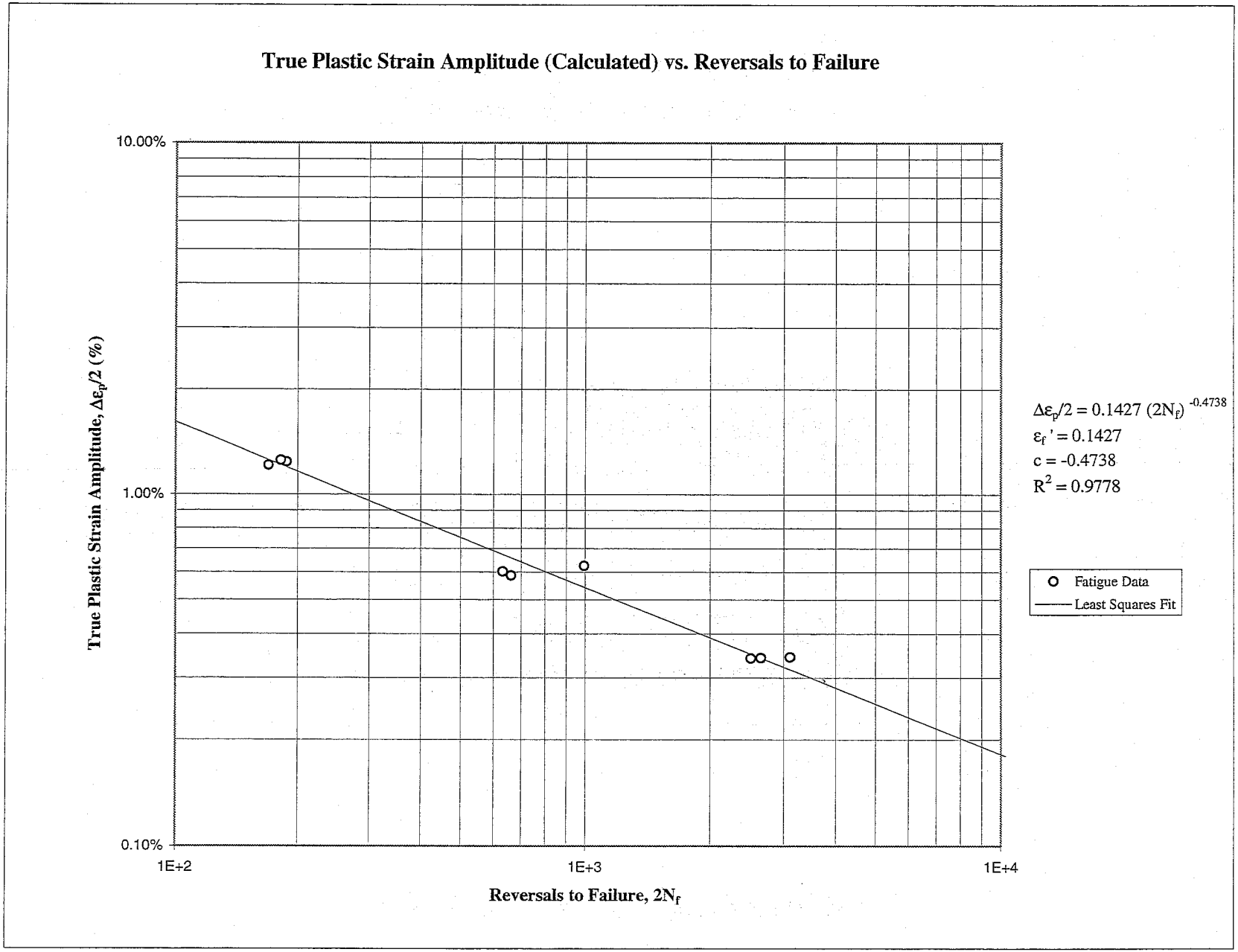

Figure 10: Calculated true plastic strain amplitude versus reversals to failure

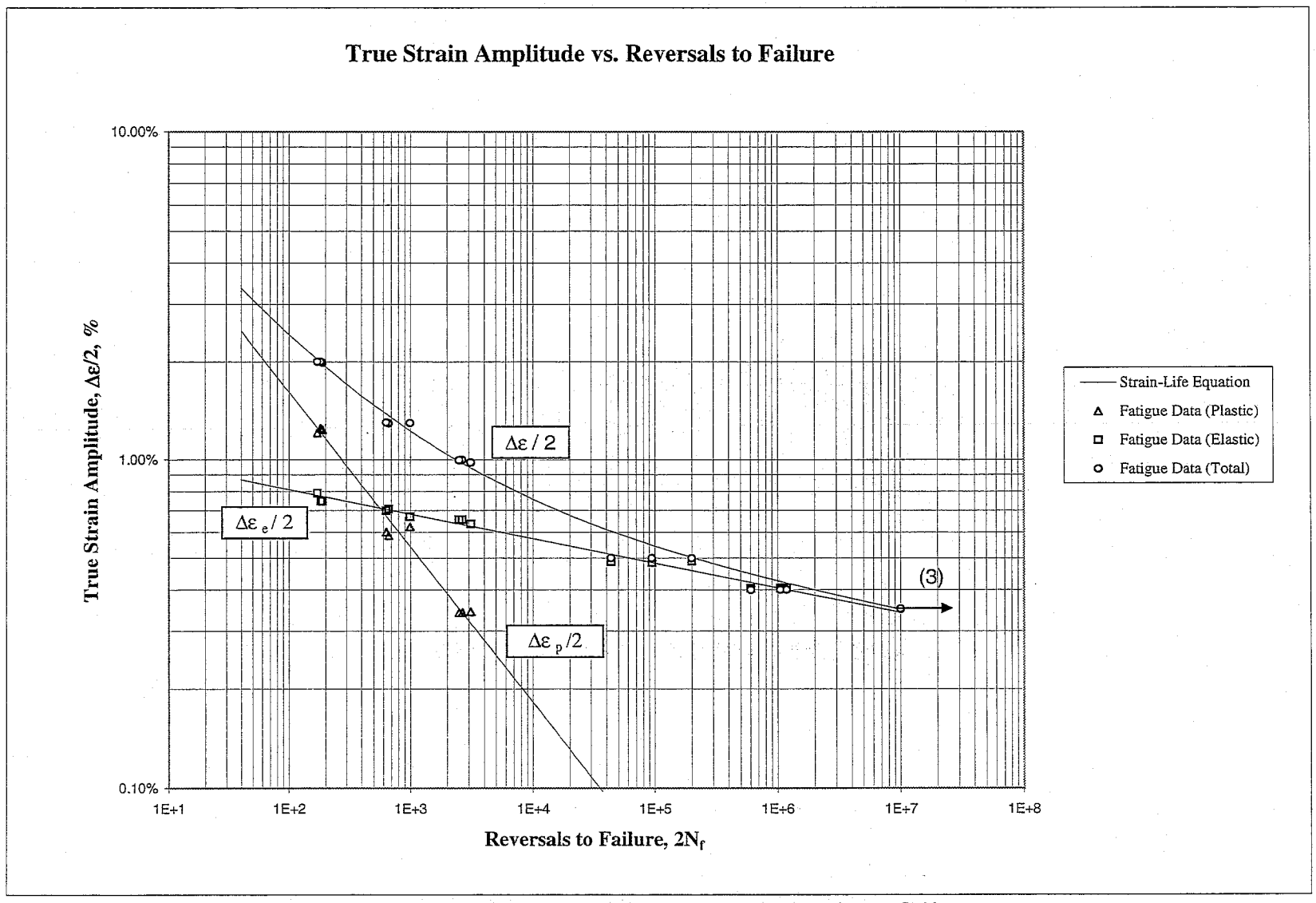

Figure 11: True strain amplitude versus reversals to failure

REFERENCES

[1] ASTM Standard E606-92, "Standard Practice for Strain-Controlled Fatigue Testing," Annual Book of ASTM Standards, Vol. 03.01, 1997, pp. 523-537.

[2] ASTM Standard E83-96, "Standard Practice for Verification and Classification of Extensometers," Annual Book of ASTM Standards, Vol. 03.01, 1997, pp. 198-206.

[3] ASTM Standard E1012-93a, "Standard Practice for Verification of Specimen Alignment Under Tensile Loading," Annual Book of ASTM Standards, Vol. 03.01, 1997, pp. 699-706.

[4] ASTM Standard E8-96a, "Standard Test Methods for Tension Testing of Metallic Materials," Annual Book of ASTM Standards, Vol. 03.01, 1997, pp. 56-76.

[5] ASTM Standard E112-96, "Standard Test Methods for Determining Average Grain Size," Annual Book of ASTM Standards, Vol. 03.01, 1997, pp. 227-249.

[6] ASTM Standard E45-97, "Standard Test Methods for Determining the Inclusion Content of Steel," Annual Book of ASTM Standards, Vol. 03.01, 1997, pp. 157-170.

[7] ASTM Standard E739-91, "Standard Practice for Statistical Analysis of Linear or Linearized Stress-Life (S-N) and Strain-Life (ε-N) Fatigue Data," Annual Book of ASTM Standards, Vol. 03.01, 1995, pp. 615-621.

[8] ASTM Standard E646-93, "Standard Test Method for Tensile Strain-Hardening Exponents (n-values) of Metallic Sheet Materials," Annual Book of ASTM Standards, Vol. 03.01, 1997, pp. 550-556.

[9] Bridgman, P. W., "Stress Distribution at the Neck of Tension Specimen," *Transactions of American Society for Metals*, Vol. 32, 1944, pp. 553-572.

[10] Khalil M., and Topper T. H., "Fatigue Behavior, Monotonic Properties and Microstructure Data for 4320, Caburized (Case) Steel (Iteration No. 50)", July 2002.

APPENDIX

Table A.1: Summary of monotonic tensile test results

Specimen ID	D_o, mm (in.)	D_f, mm (in.)	L_o, mm (in.)	L_f, mm (in.)	E, GPa (ksi)	YS (offset=0.2%), MPa (ksi)	UYS, MPa (ksi)	LYS, MPa (ksi)	YPE, %	S_u, MPa (ksi)	K, MPa (ksi)	n	%EL, %	%RA, %	R, mm (in.)	σ_f *, MPa (ksi)	ε_f
F2-24	5.07 (0.200)	3.33 (0.131)	7.62 (0.30)	10.19 (0.40)	202.1 (29,316.0)	1335.9 (193.8)	NA	NA	NA	1692.2 (245.4)	2331.8 (338.2)	0.0842	33.7%	56.9%	2.20 (0.087)	2184.2 (316.8)	84.1%
F2-25	5.11 (0.201)	3.46 (0.136)	7.62 (0.30)	9.93 (0.39)	200.2 (29,036.4)	1353.1 (196.3)	NA	NA	NA	1718.5 (249.2)	2355.8 (341.7)	0.0838	30.3%	54.2%	2.90 (0.114)	2211.3 (320.7)	78.0%
Average values	5.1 (0.200)	3.39 (0.134)	7.62 (0.30)	10.06 (0.40)	201.2 (29,176.2)	1344.5 (195.0)	NA	NA	NA	1705.3 (247.3)	2343.8 (339.9)	0.0840	32.0%	55.5%	2.55 (0.100)	2197.8 (318.7)	81.1%

* The values of true fracture strength are corrected for necking according to the Bridgman correction factor.

Table A.2: Summary of constant amplitude completely reversed fatigue test results

Specimen ID	Test control mode	Test freq., Hz	E, GPa (ksi)	At midlife ($N_{50\%}$)						$2N_{50\%}$, [a] reversals	$(2N_f)_{50\%}$, [b] reversals	Failure location [c]
				E', GPa (ksi)	$\Delta\varepsilon/2$, %	$\Delta\varepsilon_p/2$ (calculated), %	$\Delta\varepsilon_p/2$ (measured), %	$\Delta\sigma/2$, MPa (ksi)	σ_m, MPa (ksi)			
F2-4	strain	0.10	202.6 (29,380.0)	185.3 (26,874.0)	1.984%	1.237%	1.180%	1503.2 (218.0)	-34.3 (-5.0)	128	188	IGL
F2-9	displacement	0.10			2.000%	1.251%		1507.5 (218.6)	-24.4 (-3.5)		182	IGL
F2-29	displacement	0.10			2.000%	1.209%		1591.1 (230.8)	-85.1 (-12.3)		170	IGL
F2-6	strain	0.20	203.2 (29,470.0)	186.6 (27,059.7)	1.294%	0.586%	0.537%	1423.9 (206.5)	-34.4 (-5.0)	374	662	IGL
F2-13	displacement	0.20			1.300%	0.602%		1405.1 (203.8)	9.3 (1.3)		632	IGL
F2-27	strain	0.20	198.9 (28,840.0)	182.7 (26,492.3)	1.295%	0.624%	0.558%	1348.5 (195.6)	-21.9 (-3.2)	512	994	IGL
F2-1	strain	0.50	204.8 (29,700.0)	192.2 (27,873.7)	0.980%	0.343%	0.319%	1280.9 (185.8)	-31.0 (-4.5)	1,602	3,106	IGL
F2-3	strain	0.50	200.6 (29,090.0)	188.5 (27,332.7)	0.998%	0.342%	0.299%	1319.5 (191.4)	-34.8 (-5.0)	1,024	2,646	IGL
F2-26	strain	0.50	202.9 (29,430.0)	189.0 (27,413.6)	0.997%	0.341%	0.299%	1320.1 (191.5)	2.6 (0.4)		2,504	IGL
F2-2	strain	2.0	204.6 (29,680.0)	203.2 (29,466.1)	0.500%	0.012%	0.018%	980.9 (142.3)	27.9 (4.0)	18,994	43,600	IGL
F2-7	strain load	2.0 5.0	205.5 (29,800.0)	203.5 (29,512.3)	0.500%	0.009%	0.018%	985.9 (143.0) 985.9 (143.0)	113.4 (16.4) 0.0 (0.0)	3,074	199,624	IGL[ss]
F2-5	strain load	2.0 5.0	202.9 (29,430.0)	202.2 (29,328.6)	0.500%	0.015%	0.019%	975.5 (141.5) 975.5 (141.5)	49.6 (7.2) 0.0 (0.0)	38,460	94,164	IGL[ss]
F2-28	strain load	2.0 20.0	203.9 (29,570.0)	204.3 (29,633.5)	0.400%	0.000%		813.7 (118.0) 813.7 (118.0)	-3.8 (-0.5) 0.0 (0.0)	4,244	602,530	IGL[ss]
F2-12	load	20.0			0.400%	0.000%		815.5 (118.3)	3.3 (0.5)		1,047,652	IGL[ss]
F2-11	load	20.0			0.400%	0.000%		816.4 (118.4)	3.3 (0.5)		1,180,590	IGL[ss]
F2-8	strain load	2.0 25.0	205.2 (29,760.0)	206.0 (29,872.1)	0.349%	0.000%		718.5 (104.2) 104.2 (718.3)	53.6 (7.8) 0.0 (0.0)	4,214	>10,000,000	No Failure
F2-10	load	20.0			0.350%	0.000%		718.5 (104.2)	0.0 (0.0)		>10,000,000	No Failure
F2-15	load	26.0			0.350%	0.000%		718.3 (104.2)	0.0 (0.0)		>10,000,000	No Failure

[a] $N_{50\%}$ is defined as the midlife cycle (for run-out tests, data is taken from the stable cycle indicated).
[b] $(N_f)_{50\%}$ is defined as 50% load drop.
[c] IGL = inside gage length; SS = subsurface cracking (location as shown in the graph below with the hardness profile).

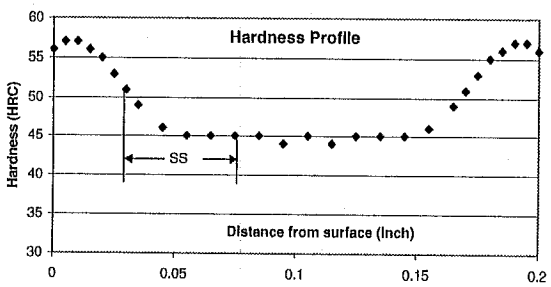

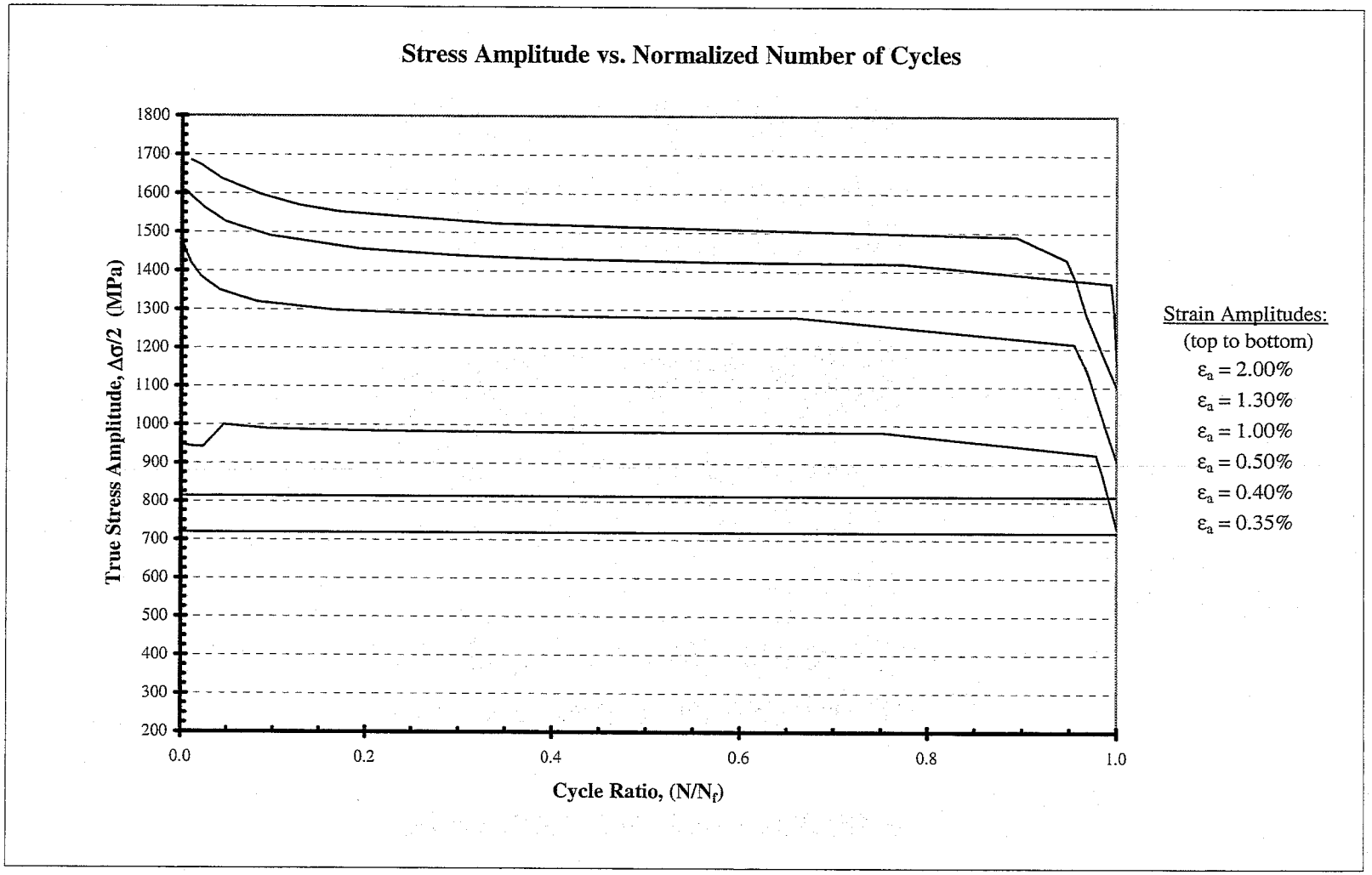

Figure A.1a: True stress amplitude versus normalized number of cycles

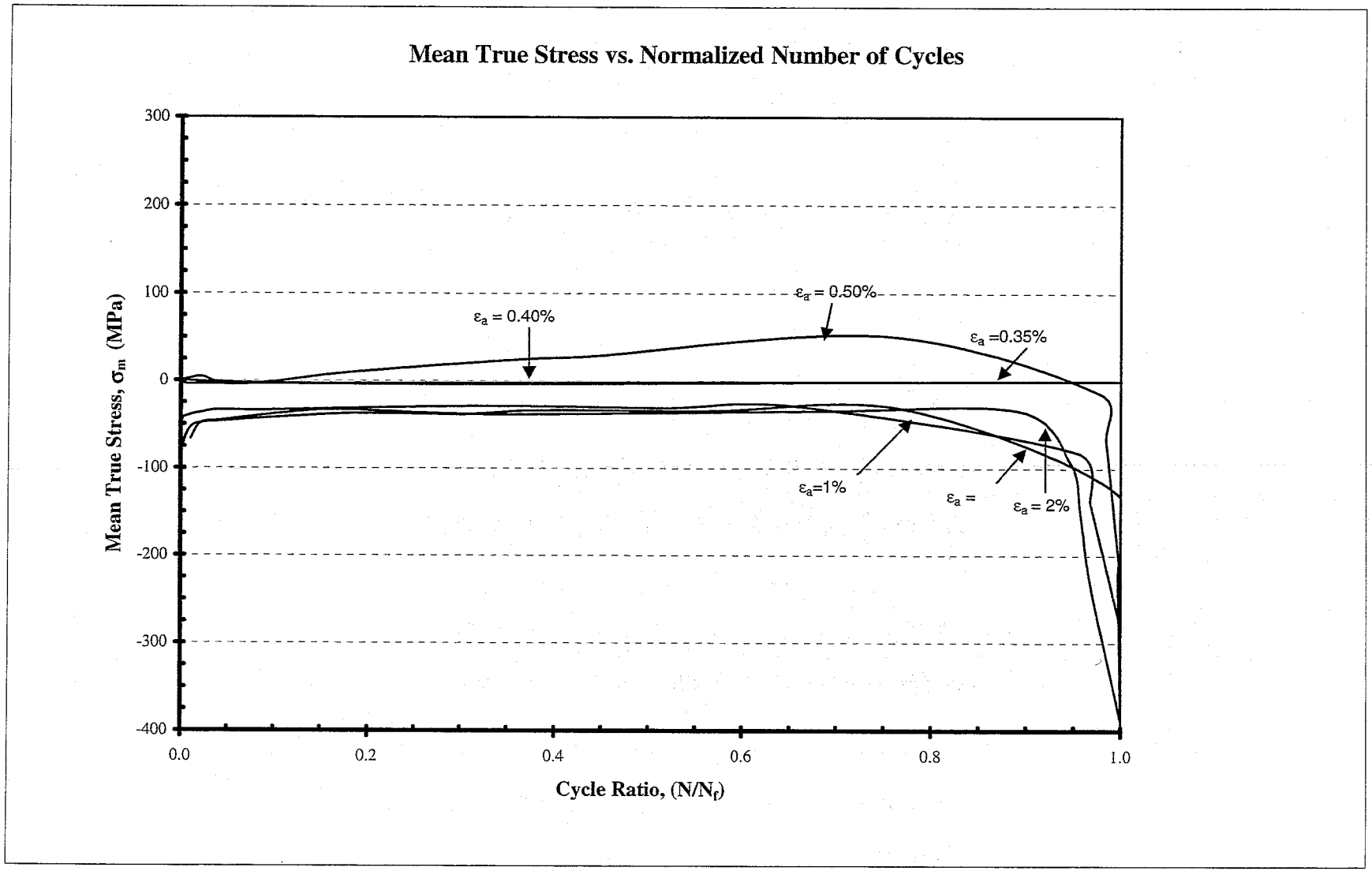

Figure A.1b: Mean True Stress versus normalized number of cycles

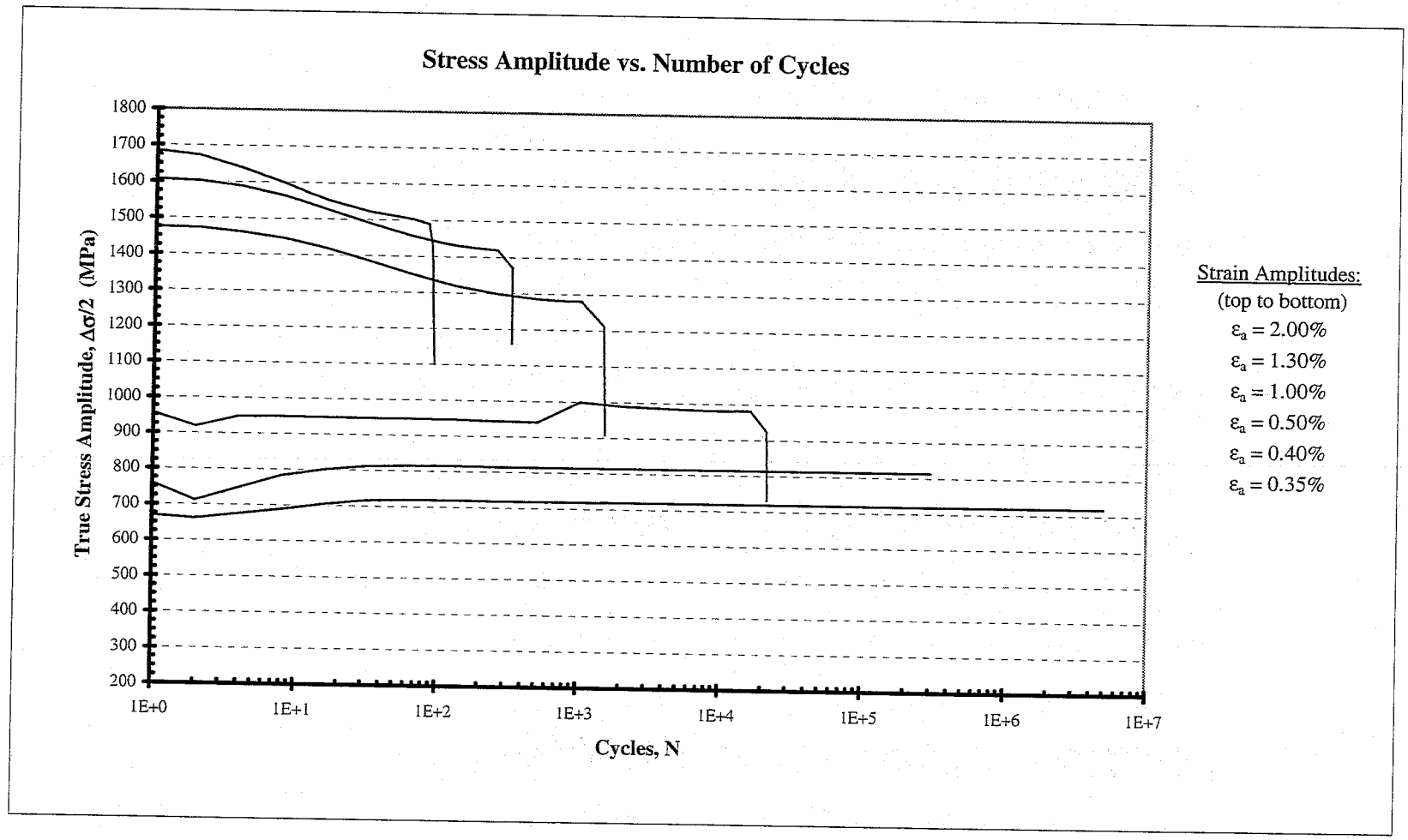

Figure A.1c: True stress amplitude versus number of cycles

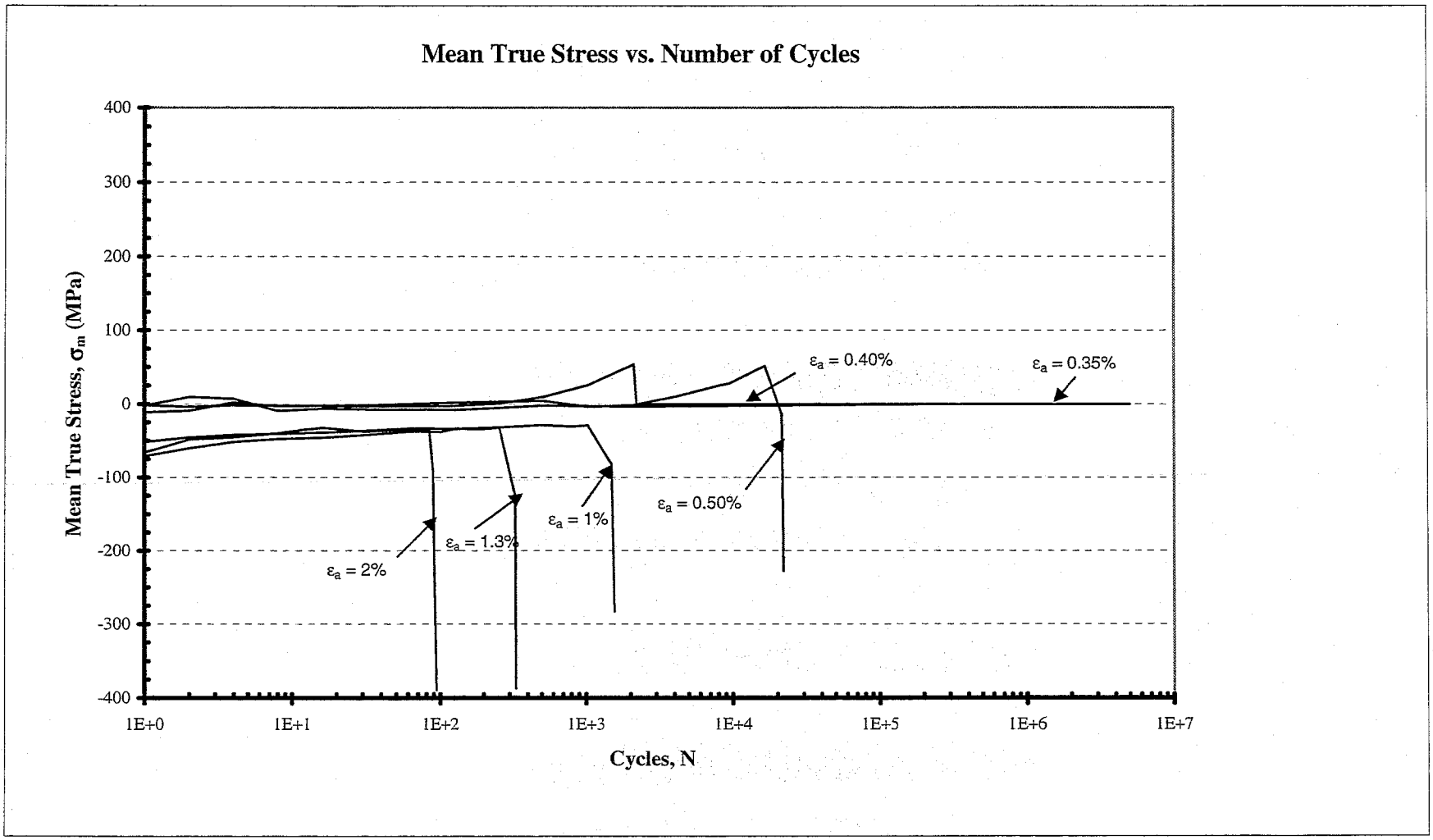

Figure A.1d: Mean True Stress versus number of cycles

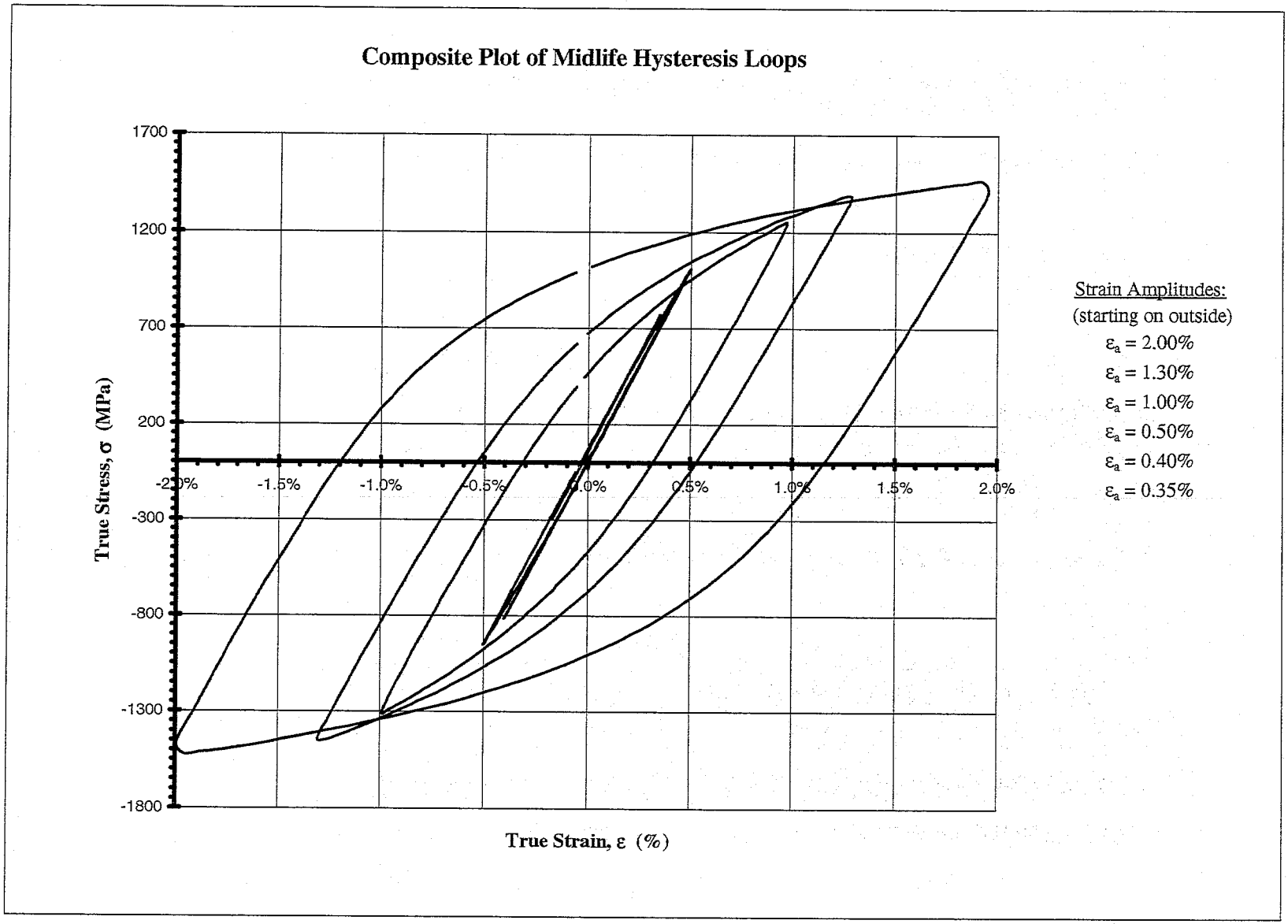

Figure A.2: Composite plot of midlife hysteresis loops

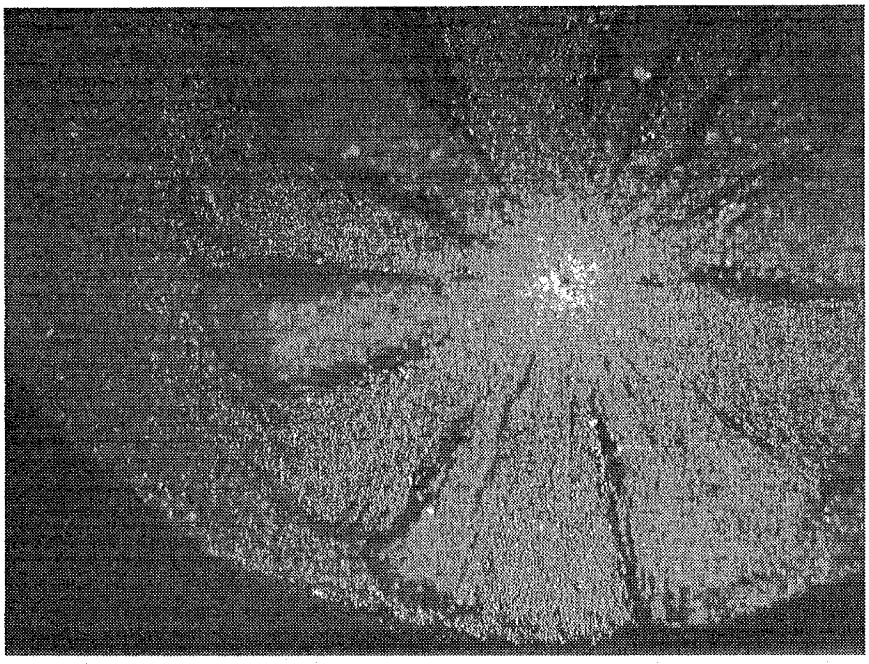

Figure A.3a: A typical subsurface failure at 50 X
for SAE 4320 Case-Core Composite steel

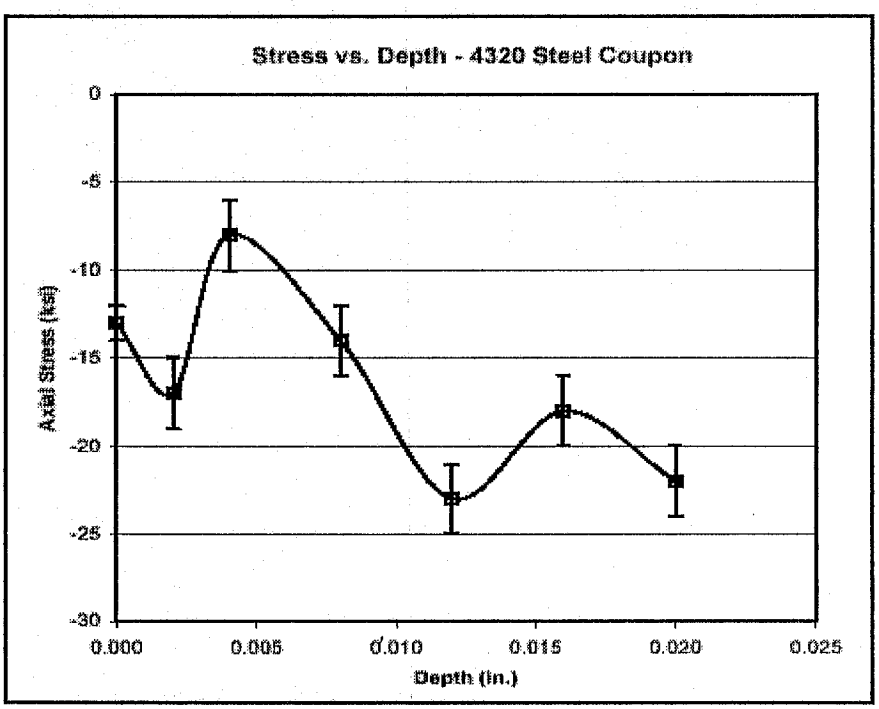

Figure A.3b: Residual stress profile (axial direction)
for SAE 4320 Case-Core Composite

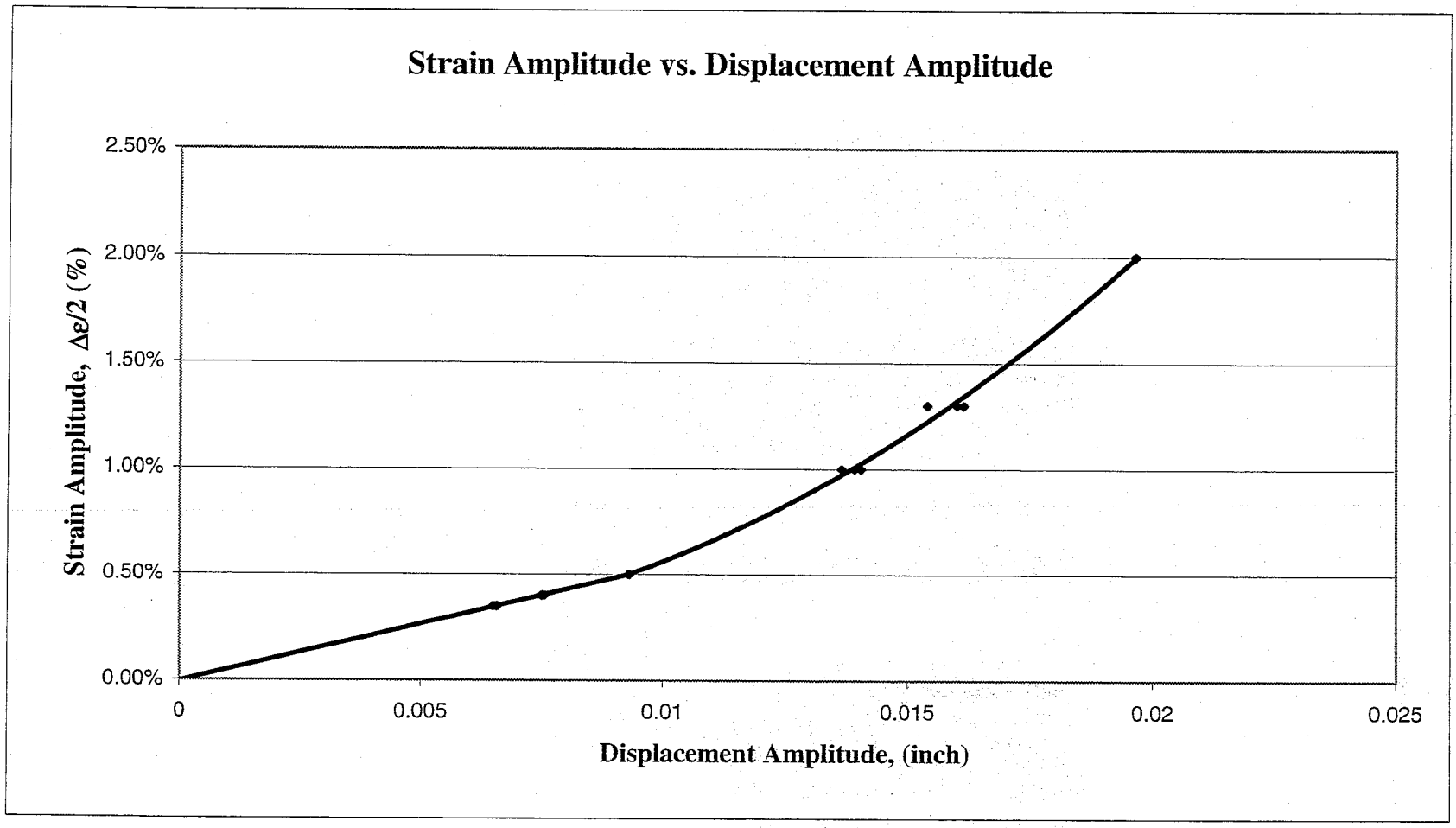

Figure A.4 Strain amplitude versus displacement amplitude

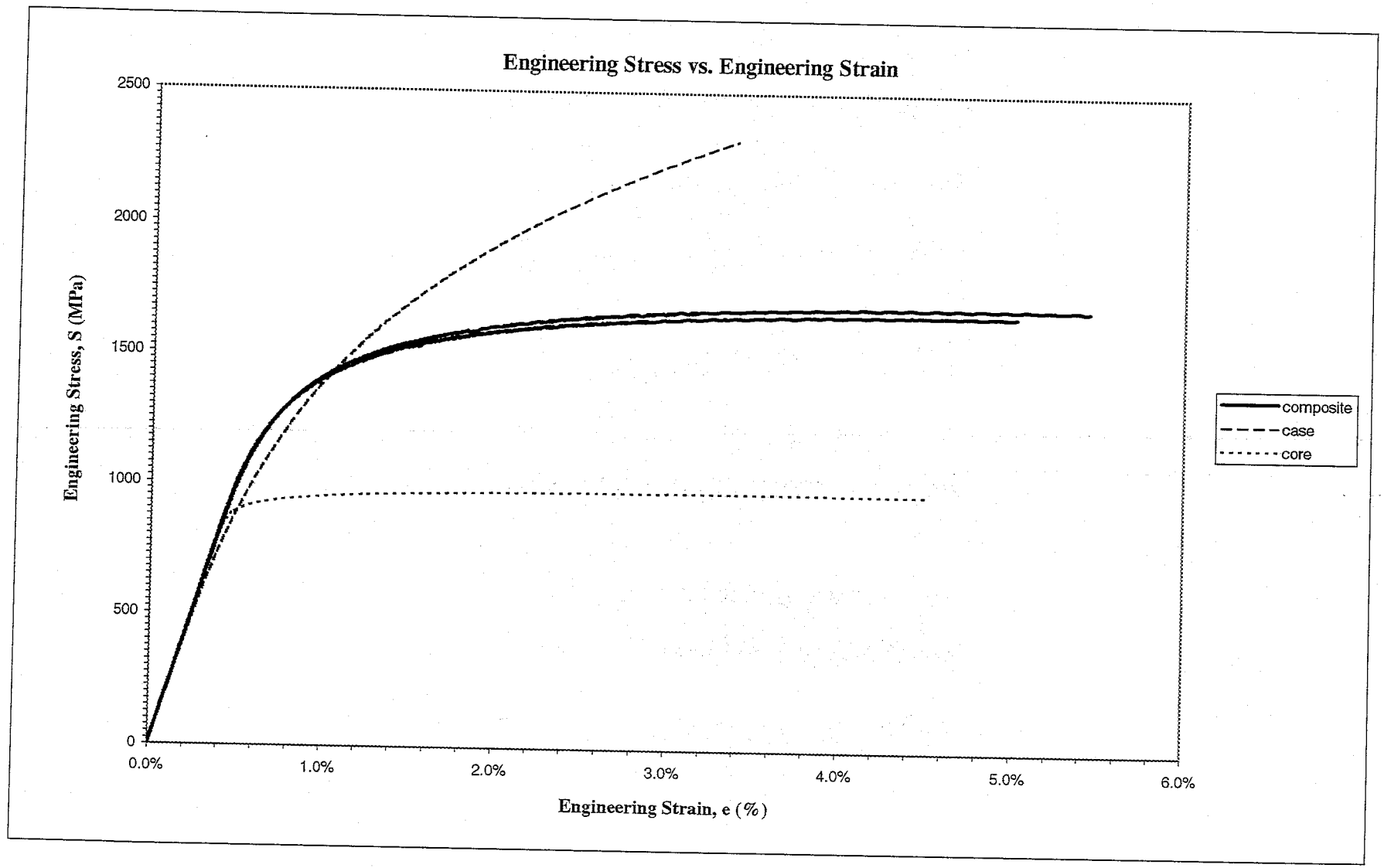

Figure A.5: Monotonic stress-strain curves
(stress-strain curves for case and core materials were obtained from U. of Waterloo reports)

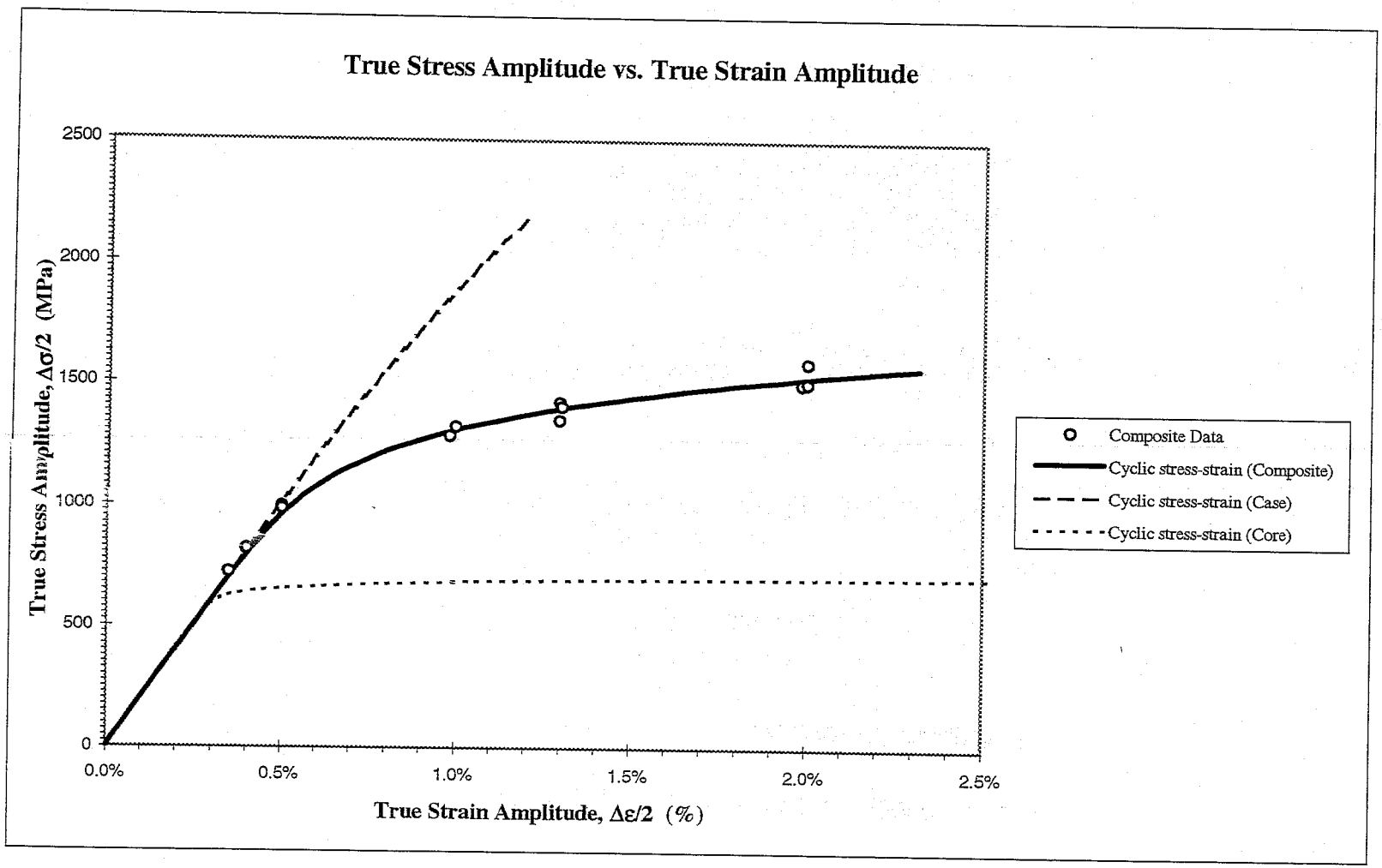

Figure A.6: True stress amplitude versus true strain amplitude

(stress-strain curves for case and core materials were obtained from U. of Waterloo reports)

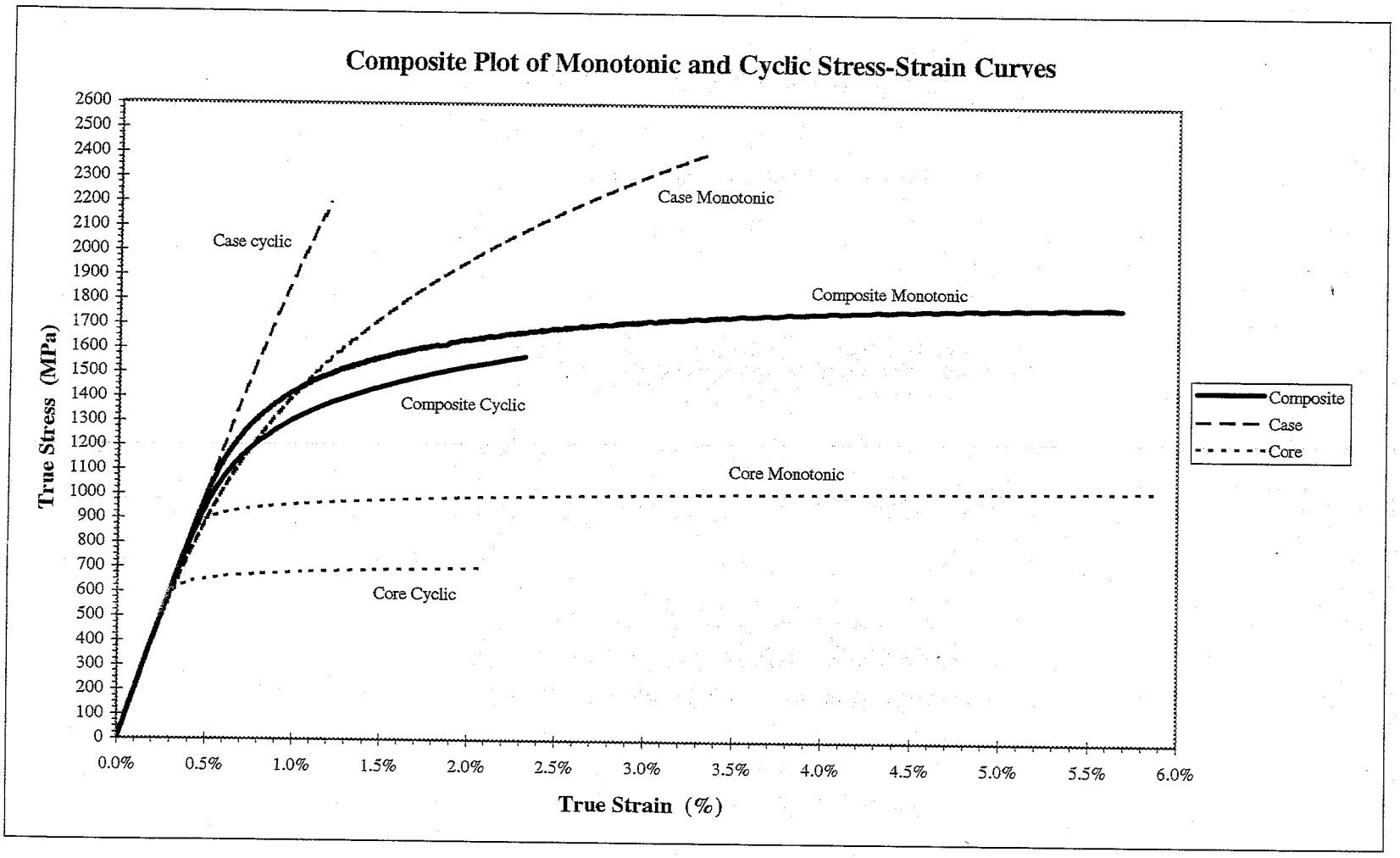

Figure A.7: Composite plot of cyclic and monotonic stress-strain curves
(Monotonic and cyclic curves for case and core materials were obtained from U. of Waterloo reports)

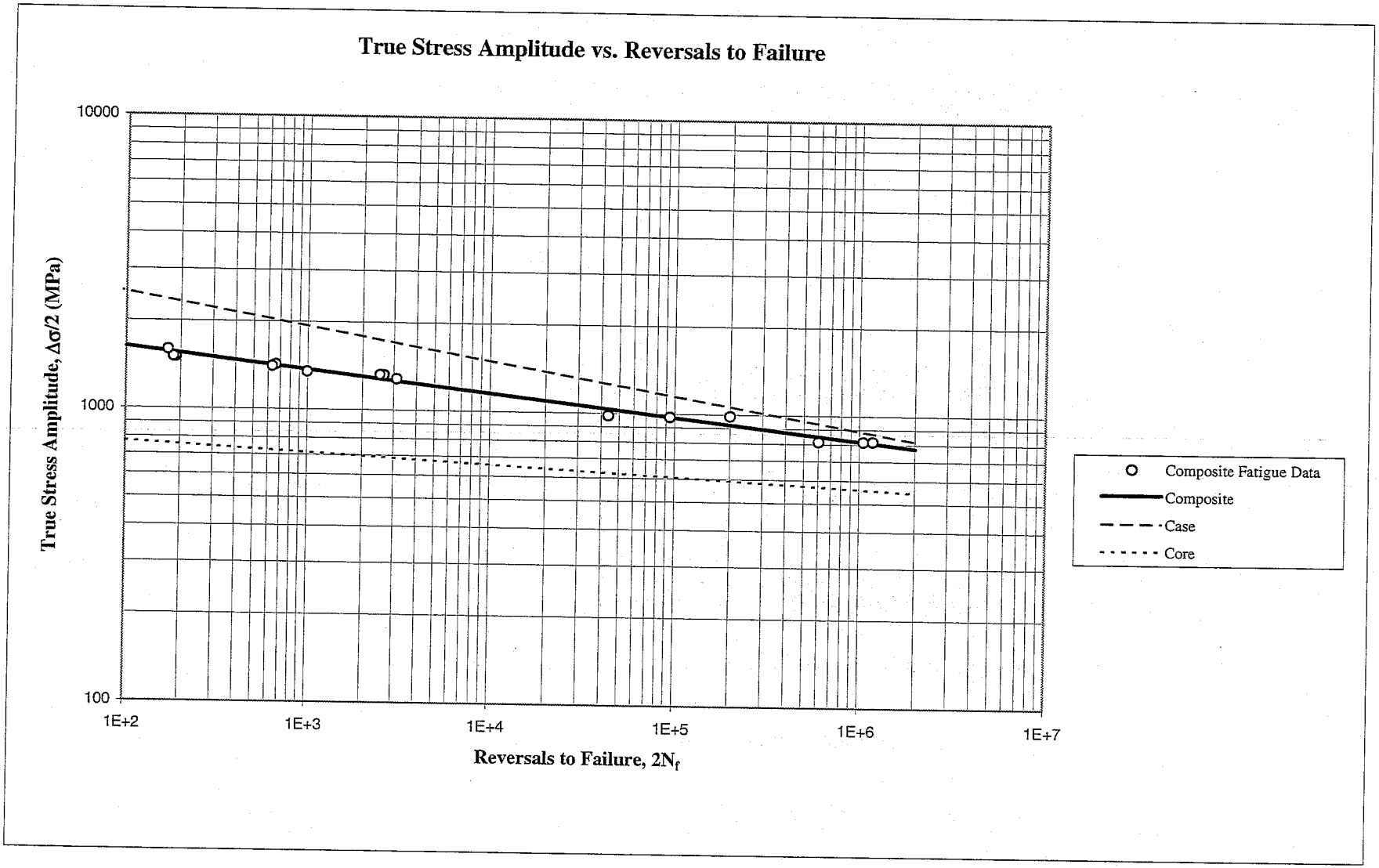

Figure A.8: True stress amplitude versus reversals to failure
(curves for case and core materials were obtained from U. of Waterloo reports)

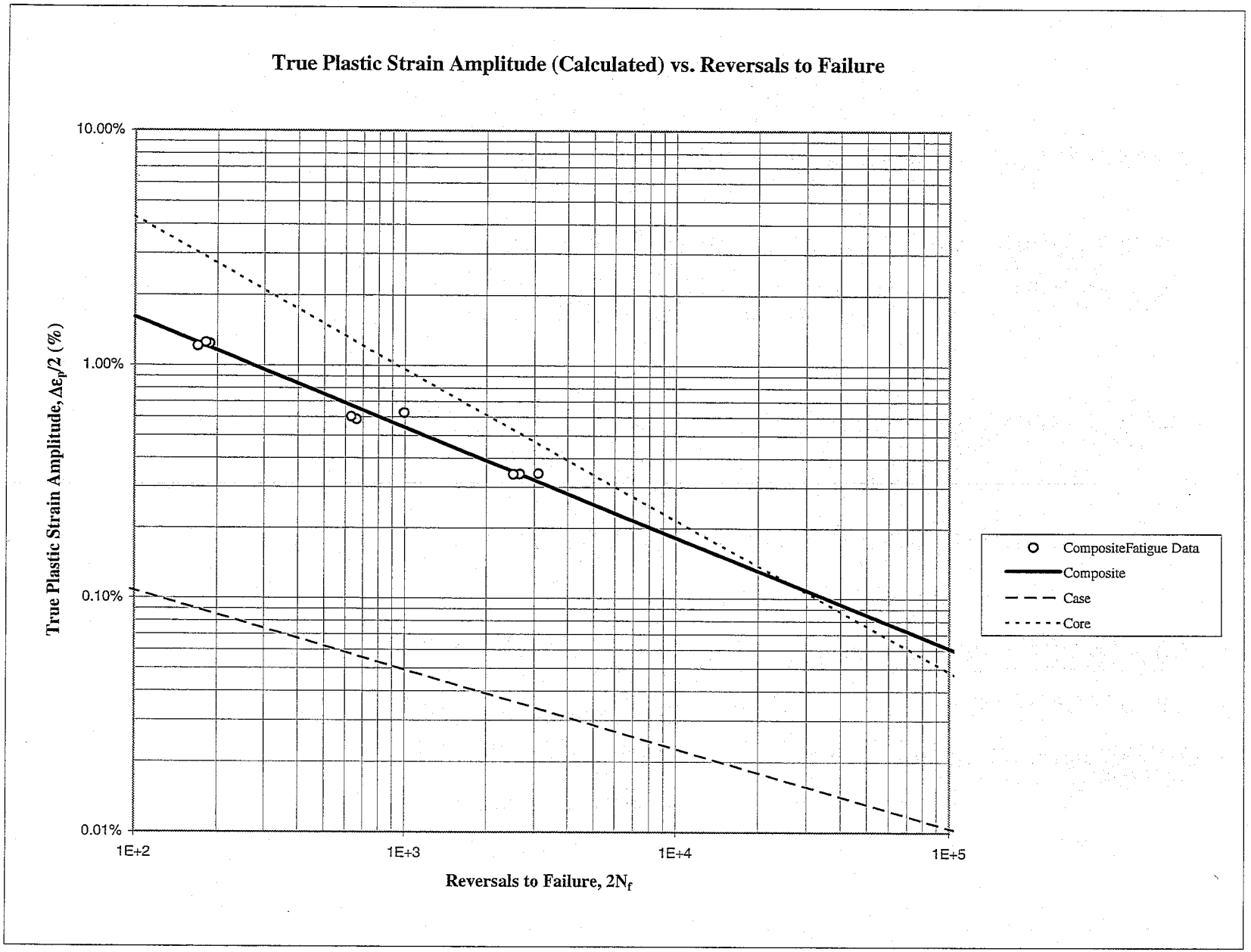

Figure A.9: Calculated true plastic strain amplitude versus reversals to failure (curves fro case and core materials were obtained from U. of Waterloo reports)

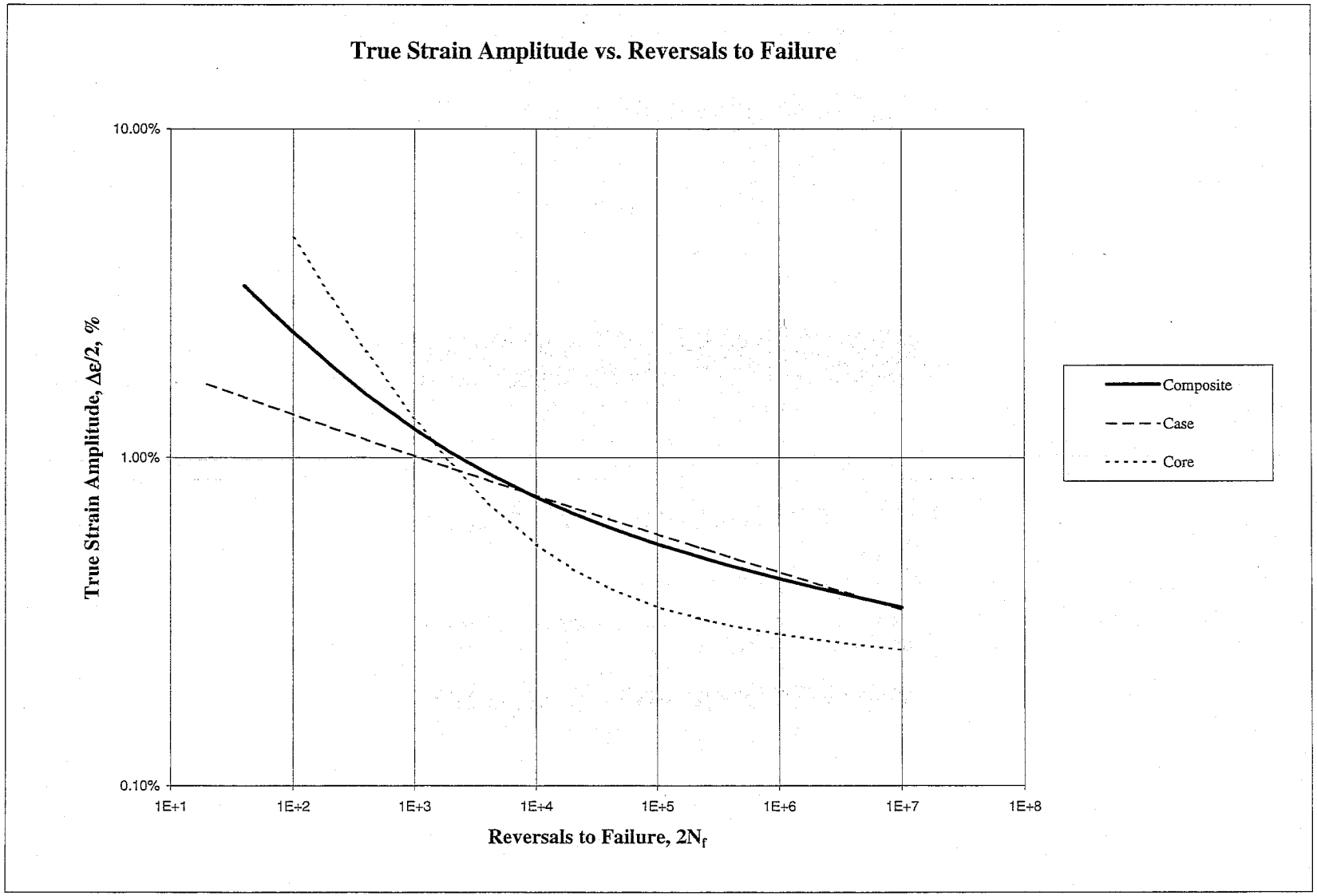

Figure A.10: True strain amplitude versus reversals to failure
(curves for case and core materials were obtained from U. of Waterloo reports)

DAIMLERCHRYSLER

Materials Engineering Lab Report
LTR Number: 115961

To:	**Peter Bauerle**	**Phone:**	**776-7387**
Location:	**CTC**		
From:	**Mechanical Properties Metallography**	**Completed:**	**5/6/2003**

Subject/Part Name: Fatigue Specimen
Report Status: Complete
Originator: Peter Bauerle
Originator Phone: 248-576-7387
Number of Parts: 1
Nature of Work: Process/Materials Development
Vendor:
Plant:
P/N:
MS: MS-7047
PS: N/A

History of Part

The sample is an attempt to develop a case/core composite fatigue specimen (iteration 63). The samples were carburized at 1700F in a 0.9% carbon potential and then stepped down to 1550F prior to quenching in fast oil at 150F. The sample was then tempered at 400F.

Test Results

Mechanical Properties - 115961

Hardness - Micro (Performed By: Kurt Snyder)

Traverse Distance (inches)	Hardness (Rockwell HRC, transcribed from microficial)
0.005	57
0.010	57
0.015	56
0.020	55
0.025	53
0.030	51
0.035	49
0.045	46
0.055	45
0.065	45
0.075	45
0.085	45
0.095	44
0.105	45
0.115	44

Hardness - Rockwell (Performed By: Kurt Snyder)

Surface Hardness: 55.8, 55.0, 57.1 Ave – 56.0 HRC

Metallography - 115961

General Microstructure Description (Performed By: Janice Bailey)

The submitted fatigue specimen (labeled iteration 63) was sectioned longitudinally, mounted, polished, and then etched in 3% Nital to reveal the microstructure. Examination using light microscopy revealed the typical case structure as tempered martensite. In addition, the case appeared to have a small amount of transformation products randomly dispersed throughout and an intergranular surface network of oxidation to a depth of 0.0004". Also, a small amount of retained austenite was noted in the case. The core structure appeared to consist of tempered martensite and carbides.

Digital image photos of both case and core at 100X and 500X taken with the Reichert-Jung MEF3 Metallograph are included in this report to document the test results.

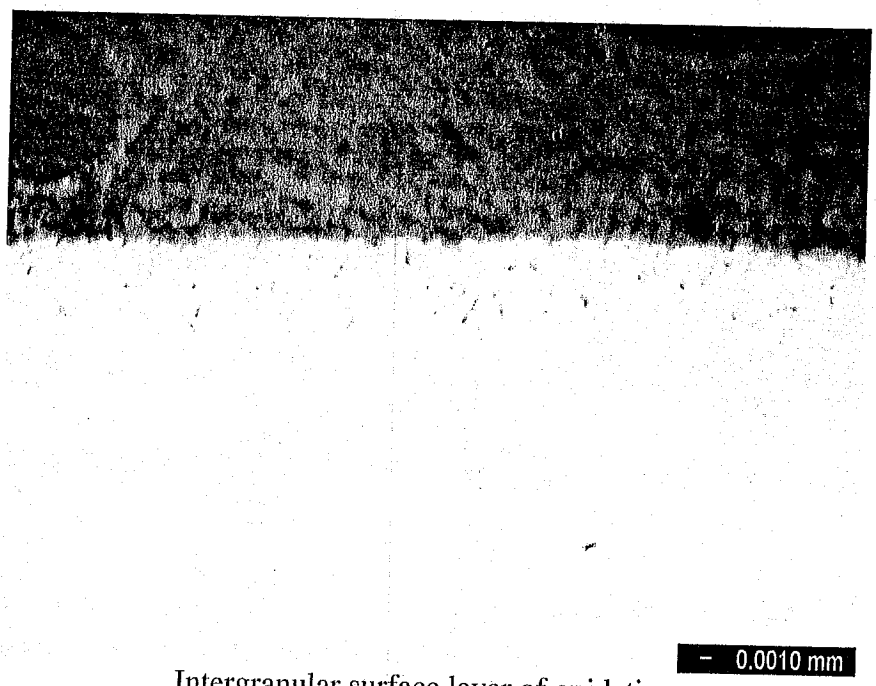

Intergranular surface layer of oxidation

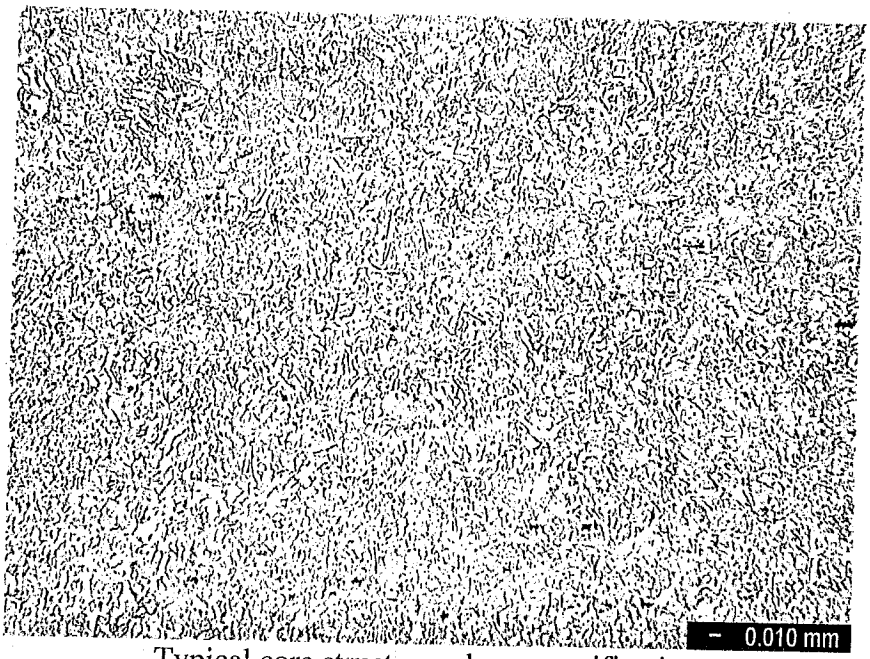

Typical core structure – low magnification

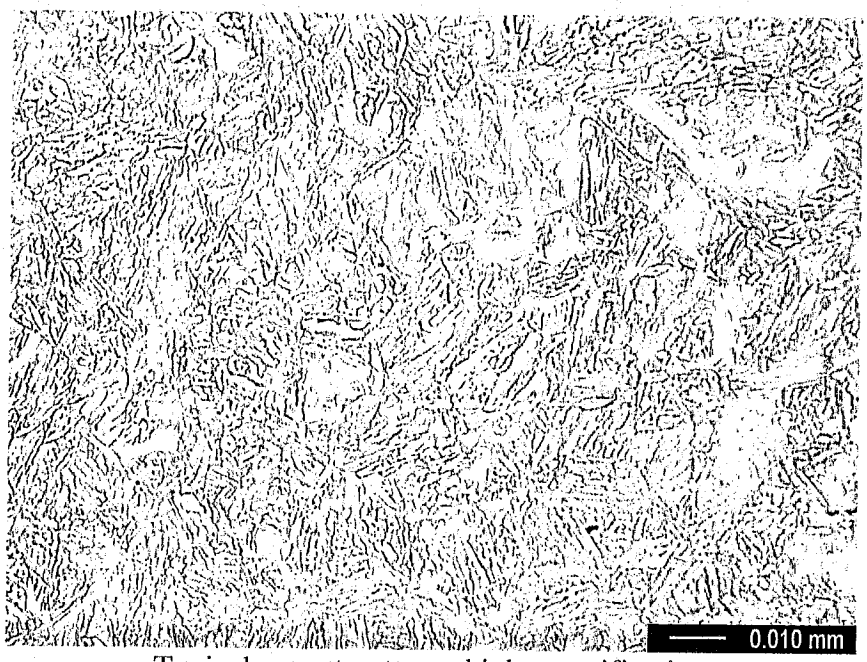

Typical core structure – high magnification

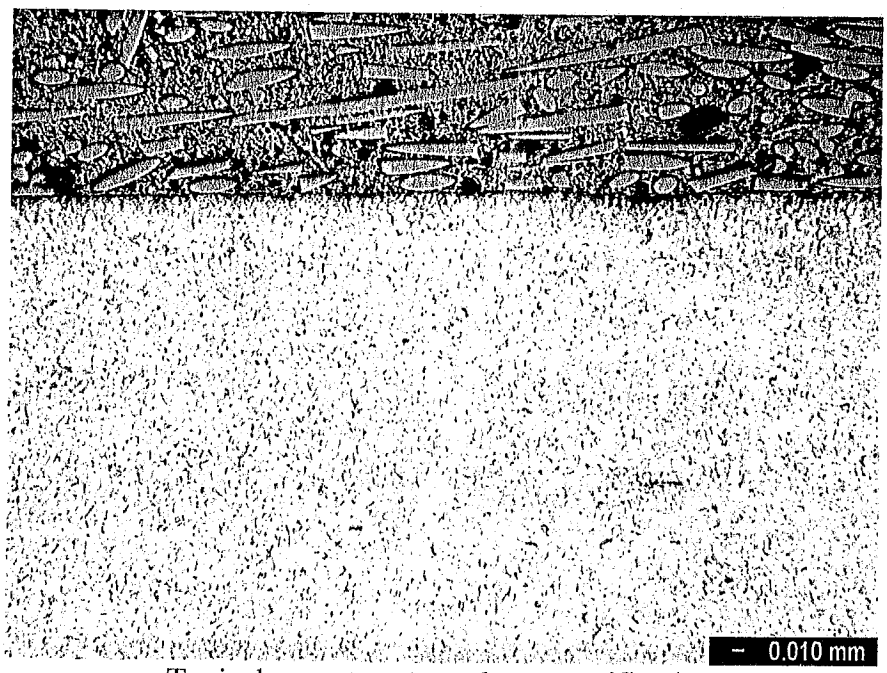

Typical case structure – low magnification

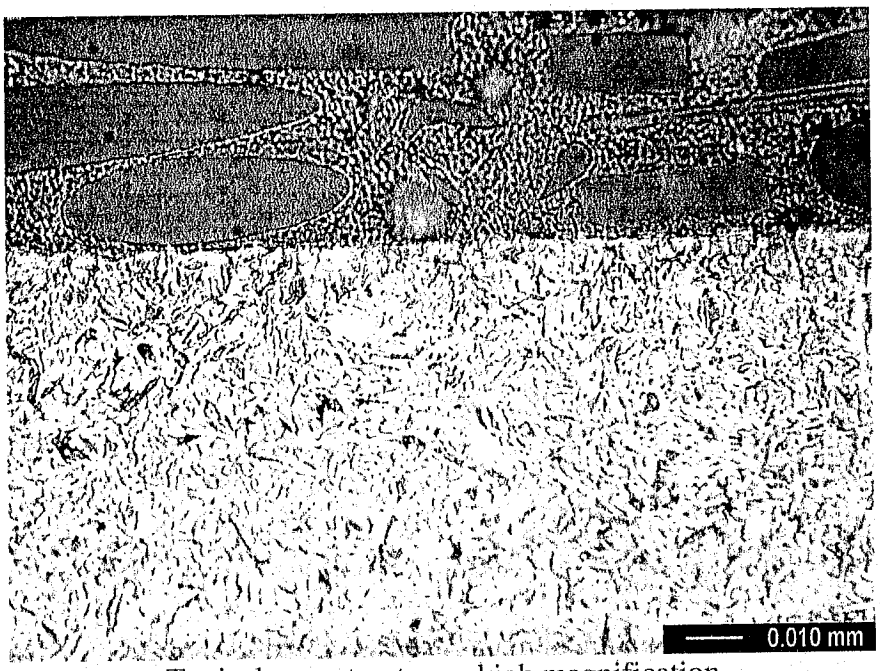

Typical case structure – high magnification